LASER SCINTILLATION PROPERTIES IN THE MARINE BOUNDARY LAYER

Arthur Frederick Schroeder

NAVAL POSTGRADUATE SCHOOL
Monterey, California

THESIS

LASER SCINTILLATION PROPERTIES

IN THE MARINE BOUNDARY LAYER

by

Arthur Frederick Schroeder, Jr.

Thesis Advisor: A. W. Cooper

December 1973

Approved for public release; distribution unlimited.

Laser Scintillation Properties

in the Marine Boundary Layer

by

Arthur Frederick Schroeder, Jr.
Lieutenant Commander, United States Navy
B.S., University of Wisconsin, 1962

Submitted in partial fulfillment of the
requirements for the degree of

MASTER OF SCIENCE IN PHYSICS

from the

NAVAL POSTGRADUATE SCHOOL
December 1973

ABSTRACT

Intensity scintillation has been studied for a He-Ne (6328A) laser beam propagating over a 4.05 kilometer horizontal path in the marine boundary layer. The results fall in three areas. (1) The covariance of the logarithm of the laser beam amplitude increases significantly with decreasing detector aperture diameter for apertures less than the first Fresnel zone size. This effect appears to be dependent on the magnitude of the refractive index structure constant, C_N. (2) The dependence of C_N on $(\text{height})^{-4/3}$ for unstable meteorological conditions was verified using the laser beam in determining C_N. (3) Frequency analysis performed on scintillation data indicates that the increase of power in higher frequencies is more dependent on the wind velocity perpendicular to the propagation path than on detector aperture diameter for apertures smaller than the first Fresnel zone size.

TABLE OF CONTENTS

I. INTRODUCTION

The structure of the atmosphere is known to modify a laser beam propagating through it. The light may be absorbed due to atmospheric gases and pollutants, scattered by molecules, electrons or particles, or undergo refraction due to turbulence caused by wind and temperature and pressure gradients. Refraction effects can be further divided into beam wander, beam spread and beam scintillation. Overall, these effects comprise a significant source of errors and distortions in laser communications, radars and control systems.

A. PROJECT HISTORY

In 1971 an interdisciplinary group of professors at the Naval Postgraduate School formed an Electro-Optics group for the purpose of pursuing advanced research in a wide variety of electro-optic areas. This group has members from Physics, Meteorology, Oceanography, Mechanical Engineering, Electrical Engineering, and Aeronautical Engineering. A team has been investigating aspects of laser beam propagation over the ocean surface under a Navy research contract. Previous theses by physics students have dealt with investigation of the modulation transfer function [Ref. 8] and with verification of the Kolmogoroff turbulence model and comparison of C_N as determined by optical methods to that determined by micro-meteorological methods [Ref. 6]. This thesis

undertakes the investigation of laser beam scintillation in the context of aperture-averaging effects, height dependence and frequency spectra. Other work being done simultaneously involves the determination of laser beam wander and beam spread [Ref. 9]. The work thus far has been with 6328 Angstrom He-Ne lasers.

B. SCINTILLATION

1. Description

Scintillation means "twinkling" or "sparkling" and is readily observable if one looks at distant astronomical bodies. The twinkling is due to changes in the refractive index of the atmosphere.

A simple model of laser beam scintillation can be described by considering the propagation path to be made up of small parcels of uniform density (and, therefore, constant refractive index). A light ray is bent slightly by each parcel, depending on the value of the parcel's refractive index, n. A slight variation in path between adjacent wave fronts causes interference patterns to be formed. The effect at a point receiver is a time varying intensity signal.

2. Theory

The inherent randomness of turbulence leads to a statistical modeling of scintillation. The refractive index variations along the propagation path modulate the intensity of a beam in a multiplicative manner; thus they modulate the

logarithm of the intensity (and amplitude) in an additive manner. The variation of the logarithm of the amplitude is, therefore, the sum of the random perturbations induced along the path. As a consequence of the central-limit theorem, the variations of the log-amplitude should follow a normal distribution.

The statistics of the turbulent mixing of the atmosphere are provided by Kolmogoroff's analysis [Ref. 1]. His theory of turbulence allows the mean square difference of the refractive index, measured at two points separated by a distance d, to be written as

$$(1) \qquad D_n(d) = \langle [n(r) - n(r+d)]^2 \rangle$$

$$D_n(d) = d^{2/3} C_N^2 \ .$$

$D_n(d)$ is called the refractive index structure function. C_N^2 is the refractive index structure constant and parameterizes the total amount of energy in the turbulence.

Tatarski [Ref. 2] has formulated the three-dimensional spectral density of the turbulence as

$$(2) \qquad \phi_n(K) = 0.033 \, C_N^2 K^{-11/3} \exp[-K^2/K_m^2] \ .$$

Here $K = 2\pi/\ell$ and is the spatial wave number corresponding to ℓ, the coherence length of a uniform turbulent parcel of air. K_m is the spatial wave number corresponding to the inner scale of turbulence, ℓ_o. This length is the lower

limit of the inertial sub-range of turbulence. For values of ℓ less than ℓ_o, viscous dissipation of energy begins to dominate. The outer scale of the inertial sub-range is L_o and corresponds to the range in which energy is added to the turbulence spectrum. The Kolmogoroff theory applies only to the region $\ell_o<\ell<L_o$. The value of ℓ_o has been estimated to be on the order of a few millimeters while L_o is on the order of meters.

The scalar wave equation is given by

$$\nabla^2 E + k^2 n^2 E = 0 \tag{3}$$

assuming that any polarization fluctuations can be neglected, and that $\lambda<<\ell_o$. λ is the wavelength of the propagating beam and k now is equal to $2\pi/\lambda$. Using Rytov's method [Ref. 3] and letting $E = \exp[\psi]$, (3) becomes

$$\nabla^2\psi + (\nabla\psi\cdot\nabla\psi) + k^2 n^2 = 0 \ . \tag{4}$$

Applying a first order perturbation of

$$\psi = \psi_0 + \psi_1$$

and

$$n = n_1 + 1$$

to equation (4) leads to

$$\nabla^2\psi_1 + 2\nabla\psi_0\cdot\nabla\psi_1 + 2k^2 n_1 = 0 \ . \tag{5}$$

The solution is

$$(6) \qquad \psi_1(\vec{r}) = 1/E_0(r) \int_{V'} 2k^2 n_1(\vec{r}_1) E_0(\vec{r}') G(\vec{r}-\vec{r}') dV' \ .$$

Working with equation (6), Schmeltzer [Ref. 4] obtained the statistical expression for the log-amplitude covariance, $C^2_{\ell A}(d)$, which Fried [Ref. 5] applies to a spherical wave propagating in a random medium with the result

$$(7) \qquad C^2_{\ell A}(d) = k^2/8\pi \ \mathrm{Re}\{ \int_0^Z ds \int_0^\infty \phi_n(K^{1/2}) \ J_0 \ (K^{1/2} ds/z) \ X \ [1 - \exp \ (Ks(z-s)/iKs] dK$$

and

$$(8) \qquad C^2_{\ell A}(d=o) = C^2_{\ell A} = 0.124 k^{7/6} Z^{11/6} C_N^{\ 2}$$

where

$$C^2_{\ell A} = \langle [\ln(A) - \ln\langle A\rangle]^2 \rangle$$

In going from (7) to (8) the assumption $\lambda^3 Z/\ell_0^{\ 4} << 1$ is made allowing the binomial expansion of the exponential and the dropping of higher order terms. This is a weak restriction at optical wavelengths.

The log-intensity covariance is then

$$(9) \qquad C^2_{\ell I} = 4 \ C^2_{\ell A}$$

which leads to

$$C_N = 1.42\, k^{-7/12} Z^{-11/12}\, C_{\ell I} \tag{10}$$

The following is a summary of the assumptions and restrictions that apply to this result:

1. The turbulence energy spectrum can be described by the empirical Kolmogoroff model (equation 1).
2. Polarization fluctuations may be neglected.
3. Only the turbulent eddies in the inertial sub-range contribute significantly to scintillation.
4. The wavelength propagated is much less than the inner scale of turbulence, ℓ_o.
5. The fluctuations in the refractive index are much smaller than the mean value.
6. $\lambda^3 Z/\ell_o^4 \ll 1$.
7. Turbulence is isotropic and homogeneous.
8. The wave propagated is spherical.
9. The detector of the intensity changes is a point detector located on the beam axis.
10. The first order perturbation technique used in the Rytov method adequately models the wave propagation.
11. The beam is propagated over a horizontal path.

II. PROBLEM

A. APERTURE AVERAGING

The basic Kolmogoroff model depends on the experimental detector being a point receiver. The general effect of having a finite detection surface is to reduce the degree of intensity fluctuations sensed, to reduce the frequency of observed changes in intensity and to increase the average signal strength.

1. Theory

For atmospheric laser propagation, the amplitude correlation distance is of the order of $(\lambda Z)^{1/2}$, the first Fresnel zone size [Ref. 2].

The first Fresnel zone is defined on the collection aperture as that radius R at which the geometric path from the source to R and from R to the detector is one-half a wavelength longer than the axial path. If the diameter of the receiving aperture is greater than $(\lambda Z)^{1/2}$ it will contain wave front sections with fluctuations of opposite sign so that the overall light flux will fluctuate weakly compared to that seen by an aperture with a diameter less than the first Fresnel zone size.

a. Wave-Optics Approach

Let I(x,y) be the light intensity. The total light flux through the aperture is

(11) $$P = \iint_A I(x,y)\, dxdy \ .$$

The fluctuations in P are defined as $P' = P - \langle P \rangle$, and

(12) $$P' = \iint_A I'(x,y)\, dxdy$$

where $I' = I - \langle I \rangle$.

The mean square fluctuations are

(13) $$\langle P'^2 \rangle = \iint_{A_1 A_2} \langle I'(x_1,y_1) I'(x_2,y_2) \rangle dx_1 dx_2 dy_1 dy_2 \ .$$

Let $$W_I = \langle I'(x_1,y_1) I'(x_2,y_2) \rangle = W_I(r)$$

where r is the distance between the two points.

Define F(x,y) such that it is zero outside the aperture and 1 on its surface. Also define

$$x = x_1 - x_2$$

$$y = y_1 - y_2 \ .$$

Equation (13) may then be written as

(14) $$\langle P'^2 \rangle = \int_{-\infty}^{\infty}\int W_I(x,y)dxdy \int_{-\infty}^{\infty}\int F(x_1,y_1)F(x_1-x,y_1-y)dx_1 dy_1 \ .$$

Now let

(15) $$H(x,y) = \int_{-\infty}^{\infty}\int F(x_1,y_1)F(x_1-x,y_1-y)dx_1,dy_1 \ .$$

Evaluating H for a circular aperture of radius R

$$F(x_1,y_1) = 1 \text{ for } x_1^2 + y_1^2 \leq R^2$$

$$F(x-x_1,y-y_1) = 1 \text{ for } (x-x_1)^2 + (y-y_1)^2 \leq R^2 .$$

The first region is a circle of radius R centered at the origin. The second is a circle of radius R centered at (x_1,y_1) so H(x,y) is the area formed by the intersection of the two circles.

$$(16) \quad H(x,y) = H(r) = 2R^2[\arccos(r/2R)-r/2R(1-r^2/4R^2)^{1/2}], r<2R$$

$$= 0, \; r \geq 2R .$$

Substituting equation (16) into (14),

$$(17) \qquad \langle P'^2 \rangle = 2\pi \int_0^{2R} W_I(r) \, H(r) \, r \, dr .$$

H(r) equals $\pi/2$ for r = 0, (point aperture), and goes to zero for r = 2R. Tatarski [Ref. 2] states that for $R<<(\lambda Z)^{1/2}$, the function $W_I(r)$ is approximately equal to $W_I(0)$ for $0 \leq r \leq 2R$. For this case

$$(18) \qquad \langle P'^2 \rangle = (\pi R^2)^2 \langle I-\bar{I} \rangle^2 .$$

Tatarski also uses the ratio

$$G(R) = \frac{Q(R)}{Q(0)}$$

where $$Q(R) = \frac{\langle P'^2 \rangle}{\langle P \rangle^2}$$

and $$Q(0) = \frac{\langle I - \bar{I} \rangle^2}{\langle I \rangle^2} .$$

The ratio G(R) shows by what factor the fluctuations of the light flux through an aperture of radius R are less than those through a vanishingly small aperture.

$$(19) \qquad G(R) = 4/\pi R^2 \int_0^{2R} W_I(r)/W_I(0)[\arccos(r/2R)$$

$$- r/2R(1-r^2/4R^2)^{1/2}]rdr .$$

G(R) equals unity for R equal to zero and monotonically decreases as R increases.

To accurately evaluate (17), the functions $W_I(r)$ and $W_I(0)$ must be known. Fried [Ref. 10] has written G(R) (his θ) in terms of $C^2_{\ell A}(r)$, the covariance of the log-amplitude.

$$C^2_{\ell A}(r) = \langle [\ell(x_1,y_1) - \langle \ell \rangle][\ell(x_2,y_2) - \langle \ell \rangle] \rangle$$

Where $\ell(x,y)$ is the log-amplitude and is related to $I(x,y)$, the intensity, by

$$I(x,y) = I_o \exp [(2\ell(x,y)]$$

As noted above, $\ell(x,y)$ is Gaussian random variable. Using his data to get values for $C^2_{\ell A}(r)$ and assuming different values for $C^2_{\ell A}(0)$, Fried calculated G(R) for normalized aperture diameters $D/(4z/k)^{1/2}$.

In the limit of the normalized aperture diameter, he predicts G(R) should vary as the inverse square of the aperture diameter.

(20) $$G(R) = D^{-2} \text{ X constant.}$$

Tatarski [Ref. 2], on the other hand, predicts

(21) $$G(R) \sim (D/2(\lambda Z)^{1/2})^{-7/3}$$

for $D >> 2\ (\lambda Z)^{1/2}$ and small values of $C_{\ell I}$ (see equations (8) and (9)).

The main restriction on this theory is that it applies to infinite plane waves for horizontal propagation paths.

b. Geometrical Optics Approach

Young, an astronomer, approached the problem using geometric optics [Ref. 11]. For an aperture much larger than the inner scale of turbulence or the diffraction scale, $(\lambda Z)^{1/2}$, geometrical optics is valid. Assuming the aperture is small compared to the outer scale of turbulence, the Kolmogoroff isotropic turbulence spectrum produces a shadow pattern with modulation power density proportional to Z^3K, where K is the spatial wavenumber. The fractional modulation power of K remaining after integration over a circular aperture of radius R is

$$f(RK) = [2J_1(RK)/RK]^2$$

where f(RK) is the aperture filter function.

The total modulation power then is

$$(22) \qquad P \sim \iint Z^3 K^{1/3} f(RK)\, K\, dK\, d\phi$$

$$= 2\pi Z^3 R^{-2} \int_0^\infty K^{-2/3}\, J_1^2(RK)\, dK \ .$$

Letting U = RK gives

$$(23) \qquad P \sim Z^3 R^{-7/3} \int_0^\infty U^{-2/3}\, J_1^2(U)\, dU = 0.66\, Z^3 R^{-7/3} \ .$$

Inspection of the integrand of equation (22) shows that it falls off rapidly for large K; most of the contribution comes from a narrow range of $K \tilde{\sim} 1/R$. Observations of stellar scintillation confirm $P \sim Z^3 R^{-7/3}$ in the large aperture range.

A surprising feature of this result is for $R = (\lambda Z)^{1/2}$

$$P \sim Z^3 [(\lambda Z)^{1/2}]^{-7/3} = \lambda^{-7/6}\, Z^{11/6}$$

the result for diffraction-limited turbulence (i.e., very small apertures). This is unexpected for a theory formulated on geometric optics.

The restriction on this theory is that R must be $>> (\lambda Z)^{1/2}$.

2. Published Experimental Data

Fried, Mevers and Keister made laser beam scintillation measurements with 21 collection apertures

ranging from one millimeter to one meter in diameter [Ref. 7]. These measurements were made with a 6328Å He-Ne laser over a sloping 8 Km path. The terrain was rolling so that the beam had an average height above the surface of greater than 15 meters. Data accumulation periods were one minute long with a time separation between data periods of four minutes. Figure 1 is a reconstruction of their data. $C_{\ell A}^2$ decreased with aperture diameter from 0.438 at 1 mm to about 0.378 at 10 mm aperture, or about 86 percent of $C_{\ell A}^2$ (1 mm). From 10 mm to 100 mm the drop was from 0.382 to 0.220 such that $C_{\ell A}^2$ (100 mm) $\simeq$ 0.557 $C_{\ell A}^2$ (10 mm). The data did not dispute Fried's theory as presented in Ref. 10 and Section A.1.a. above. His data should be evaluated in terms of possible sources of error in $C_{\ell A}^2$ measurement due to non-simultaneous receiver background compensation, and the assumption that C_N^2 was the same over the approximately one and one half hours during which the data were taken.

Young's theory [Ref. 11] has been verified in Refs. 12 and 13. This, however, applies to large apertures and stellar scintillation observations and would not be expected to apply to horizontal laser beam propagation with receiver diameters less than the first Fresnel zone size.

Kerr has reported some limited aperture averaging experiments [Ref. 14]. The data consisted of comparisons of a 32-cm receiver aperture and a 3 mm aperture at 4880 Angstroms. Kerr points out that the predicted dependence of the irradiance variance is D^{-x} for the diameter much

larger than $(\lambda Z)^{1/2}$ and that it was not observed. Different authors assign values of 2, 7/3 or 3 to X. The ratio of log-amplitude variances was plotted versus strength of turbulence as obtained from micrometeorological measurements. The ratio showed an increase from an average of 0.025 to about 0.080 as the turbulence increased with the largest data spread in the saturation region. (See Section II-C for a discussion of the saturation region.) In Ref. 15, Dunphy and Kerr presented typical ratios in comparison of a 32 cm receiver and a 6 mm receiver. The ratios were from 0.35 to 0.70 for values of C_N^2 of 5.4×10^{-13} to 3.1×10^{-12}. The ratios did not always vary consistently with C_N^2 and appear to be representative of the saturation regime.

Kerr summed up the problem of aperture averaging by saying, "An adequate theoretical description of receiver smoothing has not been given, even for nonsaturated conditions," [Ref. 14]. It should also be noted that all of the above data were collected from propagation paths over land.

B. DEPENDENCE OF SCINTILLATION ON HEIGHT, THEORY

The relationship between the refractive-index structure function, C_N^2, and micrometeorological parameters is given by

$$C_T^2 = \left(79 \times 10^{-6} \frac{P}{T^2}\right)^{-2} C_N^2 \quad . \tag{24}$$

C_T^2 is called the temperature structure parameter, P is the pressure in millibars and T is the temperature in degrees Kelvin [Refs. 6 and 16]. As temperature and pressure depend on the heights they are measured at, Wyngaard, Izumi and Collins [Ref. 16] developed a semi-empirical theory to describe the dependence of C_T^2 on height. From this theory, $C_{\ell I}^2$, as determined optically at two separate levels, can be written as a function of height.

C_T^2 may also be written as

$$C_T^2 = 3.2\ N\ b^{-1/3} \tag{25}$$

where b is the rate of molecular dissipation and N is the rate of molecular destruction of $\frac{1}{2}\langle(T-\bar{T})^2\rangle$. Surface-layer similarity theory states that statistics of the mean and turbulent flow fields, when properly made dimensionless, are universal functions of only a stability parameter. By choosing height h, the kinematic surface stress U_*^2, and the local mean potential temperature gradient $\frac{\partial\bar{\theta}}{\partial h}$ to make the statistics dimensionless and the Richardson number Ri as the stability parameter, the following relations hold:

$$F_1(Ri) = \frac{hb}{U_*^3}\ , \text{ and} \tag{26}$$

$$F_2(Ri) = \frac{N}{hU_*(\partial\bar{\theta}/\partial h)^2}\ . \tag{27}$$

Combining (26) and (27) with (25),

$$C_T^2 = h^{4/3} \left(\frac{\partial \bar{\theta}}{\partial h}\right)^2 F_3(Ri) \tag{28}$$

where

$$F_3(Ri) = \frac{3.2\ F_2}{F_1^{1/3}} .$$

The dependence of $\frac{\partial \bar{\theta}}{\partial h}$ and Ri on h must be further delineated to establish the relation between C_T^2 and h. To do this Wyngaard, et al. [Ref. 16] chose the surface temperature flux Q in place of $\frac{\partial \bar{\theta}}{\partial h}$ and the dimensionless parameter $\frac{h}{L}$ in place of Ri as the stability parameter. L is defined by

$$L = \frac{-U_*^3 \bar{T}}{kgQ} \tag{29}$$

where k is Von Karmen's constant and is approximately equal to 0.4.

During the day over land, when heat transfer is generally upward, Q is positive and $\frac{h}{L}$ is negative. These are unstable conditions, i.e., the buoyant air near the surface tends to rise. At night over land, Q is generally negative. Over the ocean surface Q may be negative, zero or positive depending on the relative temperature influence of the ocean. When Q = 0, $\frac{h}{L} = 0$; these are neutral conditions which may be approached under very cloudy conditions.

To clarify equation (28), first convert $\frac{\partial \bar{\theta}}{\partial h}$ and Ri in terms of the new variables, h, U_*, Q and L.

(30) $$\frac{hU_*}{Q}\frac{\partial\bar{\theta}}{\partial h} = -\frac{h}{T_*}\frac{\partial\bar{\theta}}{\partial h} = g_1\left(\frac{h}{L}\right)$$

and

(31) $$Ri = g_2\left(\frac{h}{L}\right)$$

where $T_* = -\frac{Q}{U_*}$. The g's are functions of $\frac{h}{L}$ only and are given in Ref. 17. Then, equation (28) becomes,

(32) $$C_T^2 = T_*^2 h^{-2/3} g_3\left(\frac{h}{L}\right) .$$

The function g_3 is given by

(33) $$g_3 = 4.9\left[1 - 7\left(\frac{h}{L}\right)\right]^{-2/3} \text{ for } 0 \geq \frac{h}{L}$$

and

(34) $$g_3 = 4.9\left[1 + 2.75\left(\frac{h}{L}\right)\right] \text{ for } 0 \leq \frac{h}{L} .$$

For unstable conditions, with $0 \geq \frac{h}{L}$ and $-\frac{7h}{L} >> 1$, (33) becomes $g_3 \simeq \frac{4}{3}\left(-\frac{h}{L}\right)^{-2/3}$ and (32) is then

(35) $$C_T^2 \simeq \frac{4}{3} T_*^2 (-L)^{2/3} h^{-4/3} .$$

For stable conditions, C_T^2 decreases with height more slowly than $h^{-2/3}$. For neutral conditions, the dependence approaches $h^{-2/3}$.

When comparing simultaneous measurements at two different heights in the surface layer the following relationship holds,

$$\frac{C_T^2(1)}{C_T^2(2)} = \left[\frac{h(1)}{h(2)}\right]^{-4/3} = \frac{C_N^2(1)}{C_N^2(2)} \quad . \tag{36}$$

For optically determined data then,

$$\frac{C_{\ell A}^2(1)}{C_{\ell A}^2(2)} = \frac{C_N^2(1)}{C_N^2(2)} = \left[\frac{h(2)}{h(1)}\right]^{4/3} \tag{37}$$

under unstable conditions. If conditions are neutral

$$\frac{C_T^2(1)}{C_T^2(2)} = \frac{C_N^2(1)}{C_N^2(2)} = \frac{C_{\ell A}^2(1)}{C_{\ell A}^2(2)} = \left[\frac{h(2)}{h(1)}\right]^{2/3} \tag{38}$$

The authors of this theory have pointed out certain restrictions to it [Ref. 16]. First of all, this is a surface layer model requiring local isotropy and may not apply at greater heights in the atmosphere. Secondly, the relationships used hold for long-term, or ensemble, averages of turbulence properties. Time averages are only approximations to ensemble averages. Thirdly, the theory is limited to horizontally homogeneous conditions. This means that a given portion of surface, with area large compared to that of a typical roughness element, looks like any other portion. This is to ensure that the flow structure is in equilibrium with the surface.

C. SATURATION REGION

1. Description

It is generally accepted in the literature that equation (7),

$$C_{\ell A}^2 = 0.124\ k^{7/6} z^{11/6}\ C_N^2$$

does not describe the refractive index structure constant for values of

$$C_{\ell A}^2 = \langle (\ln A - \ln \bar{A})^2 \rangle \geq 0.8$$

[Refs. 2, 11, 14, 15, and 18 - 21). The effect of saturation is seen in comparing $C_{\ell A}^2$ determined optically with $C_{\ell A}^2$ determined using values of C_N^2 as obtained from micrometeorological methods. A one to one relation is followed until $C_{\ell A}^2$ (optical) reaches about 0.8 where it levels off and then decreases for increasing values of $C_{\ell A}^2$ (thermal) [Refs. 14, 20 and 21].

Tatarski has investigated the effect of using the method of smooth perturbations in deriving equation (7) concluding that $C_{\ell A}^2(z) << 1$ was a limiting factor [Ref. 2].

Using a dimensional argument, Kerr deduces the relation

$$C_{\ell A}^2(\text{Maximum}) = 0.6$$

independent of wavelength, for the onset of saturation [Ref. 14].

2. Theory

DeWolf has developed a theoretical description of the behavior of $C_{\ell A}^2$ [Ref. 20]. In so doing, he points out that the Rytov approximation of smooth perturbations is really restricted by the physical condition that ray bending does not deflect rays as much as one Fresnel zone off the axis.

The region of turbulence where $C_{\ell A}^2 < 1$ is considered to generally obey equation (7), with the best application being for $C_{\ell A}^2 << 1$. The saturation region can be defined by

$$1 < K_m^{1/3} k z^2 C_N^2 << k \frac{L_o^2}{z}$$

where K_m is the spatial wave number corresponding to the inner scale of turbulence, k is the optical wave number, z is the path length and L_o is the outer scale of the inertial subrange. In this region the irradiance remains log-normal. The dependence of the log-amplitude variance $\langle dX^2 \rangle$ is calculated to be

$$\langle dX^2 \rangle = 0.41 \, (K_m^{7/3} \, z^3 \, C_N^2)^{-1/6}. \tag{39}$$

In terms of $C_{\ell A}^2$ (for a spherical wave)

$$\langle dX^2 \rangle = 0.33 \, (K_m^2 \, \frac{z}{k})^{-7/36} \, (C_{\ell A}^2)^{-1/6}. \tag{40}$$

The derivation of (39) was based on plane wave theory. In order to solve equation (39) K_m must be determined experimentally, which is difficult to do.

Other authors have attempted to model this region, but, to date, none have sufficiently satisfied experimental observations [Refs. 11, 13, and 22 - 27).

3. C_{NO} vs. C_{NT}

Because of the lack of an adequate theory to describe the saturation region it is necessary to correlate measurements of C_N as determined optically, C_{NO}, and C_N as determined by micrometeorological methods, C_{NT}. One of the long range goals of this project is to be able to predict, on a large scale, the behavior of a laser beam on the basis of meteorological measurements. The mathematical relationships for the unsaturated region over land are given by equations (10) and (24).

III. EXPERIMENTAL PROCEDURE

A. GENERAL EQUIPMENT DESCRIPTION

1. Detector Package

A detection system was designed and built to function under adverse environmental conditions and be adaptable to a variety of experimental parameters (Figure 2).

The detectors used were standard capacity type PIN-10 silicon Schottky photodiodes manufactured by United Detector Technology, Inc. These detectors provide a linear response from 10^{-12} watts to 10^{-3} watts, have an N.E.P. (1KHz - .85μ - 1Hz BW) of 10^{-12} watts, a rise time of 10 nanoseconds and a dark current of 0.5 microamperes. The units were operated in the photovoltaic mode with zero bias voltage and a large load resistance (typically 500,000 ohms). The active surface area (1.25 cm^2) was found to be non-uniform, somewhat reminiscent of photomultiplier tubes. A typical plot of relative voltage output versus position of a focused 6328 A laser beam is shown in Figure 3.

A 31 cm focal length lens was used in conjunction with a thin plate aperture which limited the field-of-view, and a 2.54 cm field lens to focus the input aperture on the photodiode. The field lens was necessary to remove a source of possible error due to either beam wander effects or tracking errors. The lens eliminated any motion of the image on the detection surface and thereby ensured a

constant responsivity from the detector. The field limiting plate aperture was placed at the focal point of the objective lens. The aperture was removable so that its size could be changed to meet the particular requirements of the experiment undertaken.

Placed immediately in front of the objective lens was a 10 A filter centered at 6328 A with a 65 percent peak transmission coefficient. The narrow band filter, along with the field limiting aperture helped reduce the effect of background radiation. The filter mounting limited the maximum effective receiver aperture to a 23 mm diameter. In front of the filter was an 18 leaf iris capable of being adjusted from 42mm to 3mm.

The main feature of the detection system was its method of background compensation. From Figure 2 it can be seen that the detection package was made up of two separate receiving paths. The laser signal was received through one path and the background radiation capable of being transmitted through the narrow band filter was received through the other. The field limiting aperture in the background sensor was horizontally offset from the optical axis so that it would not see the laser signal. A typical offset was such that the areas seen by the two receivers were separated by 1-1/2 meters at 4 kilometers. The placement of these apertures was tested in the laboratory over a path length of 280 meters prior to use in an experiment. The electronics system was then given simultaneous readings

of the laser signal and the background radiation from a field of view as nearly equivalent to that of the laser receiver as possible.

2. Electronic Components

A block diagram of the basic electronic components used is depicted in Figure 4. The voltage signals from the detector package were sent to a low noise differential pre-amplifier which subtracted the background radiation from the laser radiation, amplified the signal and sent it through a circuit box to the log-amplifier. At the circuit box the amplified signal was monitored using a microvoltmeter, and a calibration signal could be fed into the system when desired. A bias circuit was also built into the signal line. By chopping the signal at the laser every 60 seconds, for a 10 second period, the operator could see the amplified difference between the two detector signals and set the difference equal to zero. It should be noted that during daylight hours it was necessary to make adjustments to the bias control. On many occasions, the difference in background could be observed to drift, that is, the background radiation changed over short periods of time. This fact was the initial reason for using a simultaneous background compensation system as opposed to first recording the laser signal for a period of time and then recording the background, followed by a deconvolution of the two sets of data.

The log-amplifier was capable of accepting signals of 1 millivolt to 10 volts. The output was proportional to

the logarithm (base ten) of the signal so that input signals of 10 mv, 100 mv and 10 v corresponded to outputs of 200 mv, 400 mv, and 800 mv, respectively. This output was then sent to a wide band power amplifier where it was amplified by a factor of ten. From the power amplifier the signal was sent to an oscilloscope, where it was monitored, and then on to an F.M. conversion instrumentation tape recorder where it was stored.

The final data processing was done back in the laboratory where the tape recorded signal was sent to a 400 channel pulse height analyzer. Half of the analyzer storage was used to store the applicable calibration signal while the other half was used to accumulate and display the distribution of the scintillation signal. The sampling frequency was set to 16 KHz by an external trigger pulse generator.

The laser used for the aperture averaging experiment and for the lower level of the two-height experiment was a He-Ne Metrologic Model 920 providing an effective output power of 2.3 milliwatts at 6328 A. The laser was found to be stable after a half hour warm-up period. A 6mm focal length microscope lens system mounted on the laser output aperture imaged the beam on an 4cm focal length converging lens. This converging lens was adjustable in horizontal position allowing the beam to be diverged or focused at will. This provided an effective transmitter aperture of 6 mm. The laser with its associated lens systems was then mounted on a four inch channel. This channel, in turn,

was mounted on a base constructed of 3/4 inch aluminum plate in such a manner that an operator could make fine adjustments in train and elevation.

An additional laser was necessary for the two-height experiment. This laser was He-Ne, 6328 A, model S-100 manufactured by C-W Radiation and provided 0.8 milli-watts power. It was fitted with an adjustable beam spreader and was mounted on a heavy duty camera mount.

B. APERTURE AVERAGING

1. Propagation Path

The propagation path was 4.05 kilometers in length, 98 percent of which was over the ocean surface at a height of 4.9 meters (Figure 5). The laser was located on the ground level of the Monterey Holiday Inn about three meters inland from a 2.5 meter high vertical sea wall. The beach sloped gently from the sea wall about 40 meters to the ocean. The receivers were located in close proximity to a three-story building at Hopkins Marine Station. Here, the land sloped gently up from the ocean about 30 meters to the receiver site.

Data were taken on two days, 22 October and 27 October, 1973. The propagation path generally was perpendicular to the ocean wave flow. On these two days the average wave height was about one foot with three foot swells. Both days were sunny with no cloud influence. The first day had strong winds (20 knots) from the Southwest while the second day was calm with variable light winds (0 - 5 knots).

2. Data Accumulation

An earlier trial experiment across the same path indicated the need for multiple aperture data. The four apertures used did not provide a readily defineable relationship so it was decided to augment the small end of the selection with two additional apertures. Pieces of aluminum stock were machined to the outside diameters of 15, 9, 6.3, 4.8 and 3 mm with the sixth aperture being the 23 mm effective maximum aperture of the narrow band filters. All apertures were less than the first Fresnel zone, 5.08 cm. To change from one size aperture to another, the desired size aperture gauge was placed in the opening of the irises, the irises closed on them and the gauge removed. The movement of the irises was tight enough to ensure that there was no change in the opening once the size was set.

The major problem discovered in the trial experiment was that separate aperture data accumulation periods could not be correlated without the possibility of significant errors due to the change in C_N. To circumvent this problem another detection package was required to provide a continuous measurement of C_N at a fixed aperture. The detector package described in Ref. 6 was modified to match the maximum aperture size of the variable aperture unit and a suitable field limiting aperture plate was machined to match the other unit. The two packages were tested in the corridor laboratory to see if they would yield identical $C^2_{\ell I}$

using the 23 mm apertures. The systems agreed to ±1.3 percent under weak turbulence conditions by placing them side by side.

The data taken on 22 and 27 October, then, consisted of a continuous monitoring of C_N with a 23 mm aperture while varying the aperture size on the other detector package. Each complete data sequence started and ended with a run at 23 mm on the variable aperture package, taking about 14 minutes. Each run was of two minute duration with the laser signal being chopped every minute for background bias adjustment. The signals from the receivers ran through parallel electronic components to the F.M. tape recorder where they were simultaneously taped on different channels. An additional voice channel was utilized to make pertinent observations, including time calibrations for each run. Six data sequences were taken on 22 October and seven on the 27th of October.

3. Data Reduction

Back in the laboratory, the taped signals were fed into an oscilloscope for monitoring purposes and from there into the pulse height analyzer, PIP 400. The first signals recorded during each experiment were the calibration signals. These signals were 50, 100 and 200 millivolts at the input side of the log-amplifiers. They were stored on 200 channels at the PIP 400 in such a way that they could be superimposed over the log-intensity distributions after each run was accumulated on the other 200 channels.

The intensity distributions were log normal, as predicted by theory [Ref. 28]. The desired quantity was $C^2_{\ell I}$, the variance of the $[\ln (I/\langle I\rangle)]^2$ distribution. The quantity displayed on the PIP 400 was

$$a\log_{10} I = 0.434\ a\ln I = b\ln I \tag{41}$$

where a and b are constants. The full width at half maximum of a normal distribution is $X_{fl/2} = 2.345\ \sigma$. Therefore,

$$\sigma = 0.425\ X_{fl/2}\ . \tag{42}$$

Both σ and $X_{fl/2}$ are measured in units of whatever is distributed, in this application $b\ln I$. Now

$$\langle (b\ln \frac{I}{\langle I\rangle})^2\rangle = b^2\langle (\ln \frac{I}{\langle I\rangle})^2\rangle = b^2 C^2_{\ell I}\ . \tag{43}$$

To get σ in the right units, a scaling factor, S, based on the known calibration signals was used.

$$S = \frac{b[\ln I_2 - \ln I_1]}{X_2 - X_1\ (cm)}\ . \tag{44}$$

Then the variance of the distribution could be found by measuring $X_{fl/2}$ in cm and using

$$\sigma = \frac{0.425\ b\ln(I_2/I_1) X_{fl/2}(cm)}{X_2 - X_1\ (cm)} \tag{45}$$

which in turn yields

$$\frac{b\ [0.425\ \ln(I_2/I_1)X_{fl/2}]}{[X_2 - X_1]} = b\ C_{\ell I}\ ,$$

and finally,

$$(46) \qquad C^2_{\ell I} = \left[\frac{0.425\ \ln(I_2/I_1)X_{fl/2}(cm)}{X_2 - X_1\ (cm)}\right]^2$$

Each distribution, with the calibration signals superimposed, was photographed. $X_{fl/2}$ was then measured off the photograph using a vernier calipers. Maximum error introduced by this technique was ±2.7 percent. C_N was computed using equations (10) and (46).

C. TWO LEVEL EXPERIMENT

1. Combined Meteorological and Optical Effort

The purpose of this experiment was to test the theory presented in Section II.B. over the ocean surface. The same propagation path as described above was utilized for the lower level. The 2.3 mw laser and its corresponding receiver were 4.9 meters above the ocean surface. A second system using the 0.8 mw laser measured scintillation at a height of 12.3 meters, directly above the lower path.

The Research Vessel ACANIA was fitted with the meteorological instrumentation and anchored about 15 meters South of the mid-point of the propagation paths. Data were taken from 1943 to 2221 (PDST) on 18 October. The wind was from the South at 3 - 5 knots; waves were about two

feet high with two foot swells. For most of the experiment the area was covered with low clouds.

2. Data Accumulation and Reduction

a. Meteorological

This portion of the experiment was performed by members of the Meteorological Group. Meteorological instruments and measurement techniques were essentially the same as those reported in Ref. 29. An instrumentation mast was installed on the bow of R/V ACANIA. Two amplifier bridge circuits, (Sylvania GTE Thermosondes), each with two 60 ohm platinum wire sensors were mounted at 4.525 meters and 8.41 meters above the water line. C_T could then be obtained by measuring changes in the resistance difference between the two wire sensors spaced 10 cm apart. The resistance difference is proportional to the temperature difference. A voltage signal proportional to ΔT (rms) was recorded on a strip chart as a function of time.

In processing the data, raw values of ΔT (rms) were abstracted from the recorded chart. These values were then corrected for calibration errors in the nominal resistance of the platinum wires.

C_T was then calculated using

$$C_T = \text{true } \Delta T \text{ (rms)}/r^{1/3}$$

where r is the probe separation of 10 cm. From this, C_N was found using equation (24).

Stability conditions were estimated from observations of the gradient formed by the sea water temperature and air temperature sampled continuously throughout the experiment. Quartz thermometers were placed at the lower level and on the ocean surface.

b. Optical

The equipment used to receive and process the data was the same as for aperture averaging with one addition. All the electronic components were located at the lower receiver site to limit the number of operators to one. This required the use of a long coaxial cable from the upper receiver to its differential amplifier. To ensure no losses were encountered, a cable driving cathode-follower circuit was built using field effect transistors. The circuit performed the function of subtracting the background signal from the laser signal as well as driving the long cable.

The field limiting aperture plates were machined to cover a 9.15 meter diameter circle at the 4.05 Km distance. This, together with 3.7 meter beam diameter sizes at the receiver ensured that each receiver was only seeing the output of its respective laser.

Data were accumulated for an average of three minutes per run. All data reduction was accomplished in the laboratory using the same techniques as described in Section III.B.3.

D. FREQUENCY SPECTRUM ANALYSIS

Representative samples of data were chosen to compare the relative power spectra of scintillation. These samples include upper and lower level data from the two-height experiment, comparison of the two detector systems when side by side (12 cm apart), and a complete aperture averaging sequence.

The recorded scintillation signal was sent through a wave analyzer with a band-width of 10 Hz. The lower frequency limit of the analyzer was 20 Hz. Each signal was filtered at 10 Hz intervals from 20 to 100 Hz, at 100 Hz intervals from 100 to 1000 Hz, and at 1500, 2000, 3000, 4000 and 5000 Hz. The output was sent to an X-Y recorder. The power was determined by integrating the output curves with a planimeter.

IV. EXPERIMENTAL RESULTS

A. APERTURE AVERAGING

1. Preliminary Investigation

Initial investigation of the effect of aperture averaging on $C^2_{\ell A}$ using diameters smaller than the first Fresnel zone was conducted in the laboratory. The C-W Radiation 0.8 mw 6328 A laser beam, slightly diverged, was sent down a long corridor and reflected back to the receiver by a plane mirror. Total path length was 286 m. Turbulence was provided by seven large forced draft ventilators which, admittedly, was not representative of turbulent flow in the open atmosphere, but nevertheless, did produce a log-intensity distribution that proved to be normal.

Each sequence of measurements contained data taken using apertures of 3.5, 9, 18 and 23 mm. Relative values of $C_{\ell A}$ were calculated by using $C_{\ell A}$ obtained with the 3.5 mm aperture as the normalizing factor. The results of five data sequences and a composite plot are shown in Figure 6. Each data point is an average value taken from five or more 30 second sampling periods. The degree of aperture averaging found here indicated that further investigation on a full scale path was necessary.

2. Monterey Bay Experiments

a. 22 October 1973

As previously mentioned, this day was somewhat unusual in that the winds were quite strong and were from the South, i.e., over land.

The control receiver system, operated with a fixed 23 mm aperture, was used to continuously record data from 1555 to 1751 (PDST). Figure 7 is a plot of the values of $C_{\ell A}$ obtained when the variable aperture system was set to 23 mm vs. time. Only one data run provided identical values of $C_{\ell A}$ from both receiver systems. For the remainder of the runs, $C_{\ell A}$ values obtained with the variable aperture system were as much as 12 percent lower than the control system values. The average deviation was on the order of 6 percent lower. Some factors that may be responsible for this difference are beam wander, instrumental error and position of the receivers with respect to the beam axis.

Assuming that the calibration set in the laboratory was still valid leads to an investigation of a combination of beam wander and position relative to the beam axis. (Beam wander was measured at approximately 15 minute intervals by Beall and is reported in Ref. 9.) The intensity distribution of the beam in the absence of any turbulence can be considered to be Gaussian. If a detector is placed in the beam and the beam is allowed to wander randomly, the intensity differences sensed will depend on the magnitude of the beam wander. If the detector is on the original axis, the highest intensity sensed will be when the beam center is coincident with the detector and the lowest intensity will be when the beam is at its maximum excursion from the original axis. If, however, the detector

is placed at a point further off the original axis than the maximum beam wander, the maximum intensity sensed will be at one limit of the maximum beam wander and the minimum will be at the other. The intensity difference, then, will be much larger than that sensed when the detector is on the beam axis. When propagating in a turbulent atmosphere, these intensity differences are coupled with those caused by the medium inhomogeneities and increase the apparent scintillation.

On this day the position of the receivers in the beam was found to be about 0.35 m off center. The beam diameter was 2.74 m and the distance between sensors was 0.12 m. The control (i.e., reference) system was further away from the beam axis and, as shown in Figure 7, always had the larger value of $C_{\ell A}$.

Ho [Ref. 30] has shown theoretically that the variance of the log-amplitude fluctuations, $C_{\ell A}$, increases with radial distance from the axis of a laser beam when the aperture is located in the near field. The 4.05 km propagation path and 3 mm radius transmitter aperture placed the receivers in the far field. A similar effect to that described by Ho was, however, observed in the corridor laboratory under far field conditions. This effect, amplified by beam wander, appears to explain qualitatively the difference in $C_{\ell A}$ values obtained.

The purpose of the control system was to continuously monitor the changes in the atmosphere so that

the values of $C_{\ell A}$ obtained with the smaller apertures could be compared to a known reference. Because identical values of $C_{\ell A}$ were not obtained with the 23 mm apertures at the beginning and end of each sequence, a linear interpolation was carried out to obtain baseline data at intermediate times. This interpolation process consisted of comparing the difference in $C_{\ell A}$ values observed at the beginning of a sequence to the difference in $C_{\ell A}$ values observed at the end of the sequence. Define these values as $\Delta C_{\ell A}(t_1)$ and $\Delta C_{\ell A}(t_2)$, and F as the rate of change of $\Delta C_{\ell A}(t)$. Then

$$F = \frac{\Delta C_{\ell A}(t_1) - \Delta C_{\ell A}(t_2)}{t_2 - t_1}$$

The interpolated value of $C_{\ell A}(23mm)$ for the variable aperture system at a time t in the interval $t_1 \leq t \leq t_2$ would be equal to

$$C_{\ell A}(t) + [\Delta C_{\ell A}(t_1) - F(t-t_1)]$$

where $C_{\ell A}(t)$ is the value of $C_{\ell A}$ obtained with the control system at time t.

Figures 8 and 9 depict the relationships between $C_{\ell A}(D)$ as seen by the respective apertures and $C_{\ell A}(23\ mm)$ as determined by the interpolation process. These figures show that $C_{\ell A}(D)$ does not consistently increase and decrease with $C_{\ell A}(23mm)$ and that the value of $C_{\ell A}(D) - C_{\ell A}(23mm)$ is rather consistent for a given aperture.

Figure 10 is a plot of the differences between the values of $C_{\ell A}(D)$ for the respective apertures and $C_{\ell A}$ as interpolated from the 23 mm aperture measurements. The curve rises with decreasing aperture size until 4.8 mm is reached. The average value for the 3 mm aperture was slightly less than for the 4.8 mm aperture.

b. 27 October 1973

This day was sunny with very light and variable winds. The same procedures were followed as above. Figure 11 is a plot of the 23 mm values of $C_{\ell A}$ as determined by both systems. Once again, the two systems did not yield identical values. The control receiver system was closer to the average position of the beam axis. The difference in the plots may be qualitatively explained using the same arguments as in the previous section and adding the fact that the overall value of C_N was larger. (Beam wander measurements were not taken on this day.)

Some interesting visual observations of beam wander were made. The laser was first sighted in on the receiver array around 1200 (PDST) but kept drifting vertically downward. Because of the laser elevation adjustment mechanism, any vertical drift due to mechanical slippage would have caused the beam to move upward; therefore, the beam motion was due to the atmosphere. The rate of drop was about one meter per 10 minutes. The beam stabilized from about 1330 to 1530 (PDST) at which time it started to drift upward at about 0.3 meters per 10 minutes. A possible explanation

would be large scale density changes, or more likely density gradients. The sunny calm conditions were conducive to the formation of a non-dissipating warm air mass over the cooler ocean surface. This could form a density gradient with the density greater nearer the surface. The beam would then tend to bend downward. As the air above the surface cooled down later in the day, the beam would move in the opposite direction.

Figures 12 and 13 show the relationship between the aperture averaged system and the extrapolated 23 mm values. Figure 14 is a plot of the difference between the extrapolated 23 mm values and the values obtained using the various apertures versus aperture size. The shape of the curve is very similar to the one obtained from the data of the 22nd (Figure 10). The peak of the curve in Figure 14 is 2.6 times as large as the curve in Figure 10 indicating that the aperture averaging effect for apertures smaller than the first Fresnel zone may be functionally dependent on C_N.

c. Composite Data

Figures 10 and 14 show that the largest relative values of $C_{\ell A}$ were obtained when the 4.8 mm aperture was used. Based on this, it was assumed that the 4.8 mm aperture approximated a point receiver better than the other apertures used.

In order to find a relationship between aperture averaging and $C_{\ell A}$, an interpolation process, similar to that

carried out on the 23 mm apertures, was undertaken to establish a continuous set of values for $C_{\ell A}$ as seen by the 4.8 mm aperture. The ratios of $C_{\ell A}(D)/C_{\ell A}(4.8\ mm)$ were calculated, averaged for each collection aperture each day, and plotted as a function of aperture diameter in Figure 15. Values of $C_{\ell A}(D)/C_{\ell A}(1mm)$ obtained from curves published by Fried, et al. [Ref. 7] and reproduced as Figure 1 are plotted for comparison. Linear regression lines were calculated and plotted for all three data sets. The slope of the regression line for the 27 October data was steeper than those corresponding to 22 October and Fried's data. The lines cross in the vicinity of the point $C_{\ell A}(D)/C_{\ell A}$ equal to 0.93 and aperture diameter equal to 10.6 mm. Figure 16 is a plot of the absolute values of the $slope^{-1}$ vs $C_{\ell A}$ as seen by the 23 mm apertures for the regression lines plotted in Figure 15. The line was calculated using the least square method. (Fried's data were adjusted to apply to the 4.05 km path.) Using this limited amount of data a point collection aperture value of $C_{\ell A}$ could be estimated in the following manner. Entering Figure 16 with the observed value of $C_{\ell A}(23\ mm)$ yields the inverse slope to be used in Figure 15. Applying this slope in such a way as to cross through the empirically observed point of intersection of the regression lines will give a value for the ratio $C_{\ell A}(23\ mm)/C_{\ell A}$, which, in turn yields $C_{\ell A}$.

It is obvious that additional data are needed to formulate a reliable mathematical relationship between aperture diameter and $C_{\ell A}$ or C_N.

d. Frequency Spectrum

Clifford [Ref. 31] has calculated the theoretical temporal frequency spectrum, W(f), for a spherical wave. He solved the plane and spherical wave asymptotic forms in terms of $C^2_{\ell A}$, f_o and Ω

where $f_o = v/(2\pi\lambda L)^{1/2}$,

v is the wind velocity perpendicular to the propagation path, and

$\Omega = f/f_o$.

For a plane wave

$$W(f) = 0.44\ (C_{\ell A})^2_p\ (\frac{1}{f_o})(1+0.27\Omega^{4/3}),\ \Omega << 1 \tag{47}$$

$$W(f) = 1.14(C_{\ell A})^2_p\ (\frac{1}{f_o})\Omega^{-8/3},\ \Omega >> 1 \tag{48}$$

In the spherical wave case

$$W(f) = 0.245\ (C_{\ell A})^2_s\ (\frac{1}{f_o})[1+0.119\Omega^{4/3}],\ \Omega << 1 \tag{49}$$

$$W(f) = 2.81\ (C_{\ell A})^2_s\ (\frac{1}{f_o})\Omega^{-8/3},\quad \Omega >> 1 \tag{50}$$

These solutions are valid for a vanishingly small aperture.

Tatarski [Ref. 2] calculated the effect of receiver aperture averaging on the frequency spectrum for a

plane wave model. This effect shows up in an additional term multiplied on the kernal of the integral, which corresponds to a partial suppression of the normalized fluctuations. This factor is

$$(51) \qquad \left[\frac{2\,J_1\,(R\sqrt{K^2 + 4\pi^2 f^2/v^2})}{R\sqrt{K^2 + 4\pi^2 f^2/v^2}}\right]^2$$

where f is the frequency, v is the wind velocity perpendicular to the propagation path and K is the spatial wave number. For $f >> v/2\pi R$, this term is small for all K. For high frequencies the aperture averaging weakens the effect of inhomogeneities on all scales. If $f << v/2\pi R$, the factor is close to unity for $K << \frac{1}{R}$ and becomes small for $K >> \frac{1}{R}$. The contribution of large-scale inhomogeneities in the low-frequency part of the spectrum is virtually unaffected, whereas all scales which are small compared to the aperture radius are suppressed.

Relative power values for each aperture were obtained by dividing the power found at a particular frequency by that found at 20 Hz. From equations (49) and (50) it can be seen that the ratio $W(f_1)/W(f_2)$ for a vanishingly small aperture is a function of f_o, f_1, and f_2 only. The aperture dependence is contained as a multiplicative term in a first order Bessel function as shown in (51). The dependence should not be lost in taking the ratio $W(f_1)/W(f_2)$; therefore, when comparing relative power vs.

frequency plots, a difference should be detectable due to an aperture change. If the data samples were not taken simultaneously, changes in v could also contribute to any differences observed. Estimates were made of v because the propagation path could not be properly instrumented.

On 22 October, v was estimated to be 16 knots (8.24 meters/second). Defining

$$f_c = v/2\pi R \quad , \tag{52}$$

then for this day $f_c = 1.31\ (1/R)$. Here f_c(6.3 mm) = 417 Hz and f_c (23 mm) = 114 Hz. Figure 17 is a comparison plot of relative power vs. frequency for data obtained with a 23 mm aperture and for data simultaneously obtained with a 6.3 mm aperture.

For f > 500 Hz, the relative power curves in Figure 17 are converging. For most frequencies sampled, the 23 mm aperture receiver showed a smaller contribution to relative power. This is in agreement with the aperture dependence and with the previous statement that all scales of inhomogeneities which are small compared to the aperture radius are suppressed.

On 27 October the winds were light and variable. If an average value of 1 knot is assumed for v, $f_c = 0.082$ (1/R) and $f_o = 4$ Hz. The value of f_c ranges from 53 Hz for a 3 mm aperture to 7 Hz for a 23 mm aperture. Figures 18 and 19 are plots of the relative power vs. frequency

for the sequence of apertures. The plots are similar in shape to Figure 17.

Figure 18 was plotted from data received by 23 mm, 9 mm and 4.8 mm apertures. The values of f_c for v equal to 1 knot are 7 Hz, 18 Hz and 34 Hz respectively. For $f < 90$ Hz, variation with aperture size of the relative power in any frequency band is unpredictable and is probably due to slight variations in v for the different sample periods. Sample periods for the different apertures were four minutes apart. For $f > 90$ Hz, the smaller apertures show a larger contribution to relative power and the values tend to converge on each other as they approach zero at about 500 Hz. This is in agreement with Tatarski's model for $f >> f_c$. The temporal variations in v would have less effect in this region.

Figure 19 data were received by 15 mm, 6.3 mm and 3 mm apertures. The corresponding values of f_c for v equal to 1 knot are 11 Hz, 26 Hz and 55 Hz. The same behavior of the relative power vs. frequency is observed as in Figure 18 except that the region where ordering of W(f)/W(20Hz) is seen appears to be $f > 300$ Hz. It would be expected that this region would begin at a higher frequency due to the requirement that $f >> f_c$ and the values of f_c for this graph are generally larger than for the apertures used in Figure 18.

Figure 20 is a comparison of relative power vs. frequency as received by the 6.3 mm aperture on 22 October and 27 October. The values corresponding to 22 October are

seen to be consistently larger than those of 27 October. This difference is due to the significantly larger value of v for 22 October. A comparison of this figure with Figures 18 and 19 shows that the effect of v on relative power is greater than that of aperture size within the limits of these experiments.

Figure 21 is a plot of relative power vs. frequency as seen by the 23 mm apertures of the variable aperture system and the fixed aperture control system. The control system shows slightly lower values of relative power for most of the frequencies sampled.

B. DEPENDENCE OF SCINTILLATION ON HEIGHT

1. Optical Measurements

Optical measurements were taken from 1944 to 2219 on 18 October 1973 (PDST). The plot of $C_{\ell A}$ vs. time for the two levels is shown in Figure 22. Both receivers utilized a 23 mm aperture. The values obtained at the upper level for the first 40 minutes are not considered to be representative because of difficulties in maintaining the beam axis on the receiver. The large gap in upper level data from 2023 to 2105 was due to making beam adjustments. The data from 2105 to 2206 shows a definite relationship between the two levels.

Table 1 displays the average values of $C_{\ell A}$ for three different averaging periods and their relationship to the heights of the two systems. Period (a) was from 2105 to 2137; (b) from 2140 to 2206; and (c) from 2209 through 2221 (PDST).

TABLE 1

	Period (a)	Period (b)	Period (c)
$C_{\ell A}$ at h(1) = 16 ft.	0.360	0.349	0.271
$C_{\ell A}$ at h(2) = 40 ft.	0.192	0.192	0.204
$(h(2)/h(1))^{4/3}$	3.44	3.44	
$(h(2)/h(1))^{2/3}$			1.85
$C_{\ell A}^2(1)/C_{\ell A}^2(2)$	3.51	3.30	1.77

As discussed in Section II.B., during stable meteorological conditions C_T^2 (and therefore C_N^2) decreases with height more slowly than $h^{-2/3}$. Under neutral conditions the dependence approaches $h^{-2/3}$ and under unstable conditions C_T^2 varies as $h^{-4/3}$. For stable conditions with data taken simultaneously at h(1) and h(2)

$$\frac{C_T^2(1)}{C_T^2(2)} = \frac{C_N^2(1)}{C_N^2(2)} = \frac{C_{\ell A}^2(1)}{C_{\ell A}^2(2)} = \left[\frac{h(2)}{h(1)}\right]^{2/3} . \tag{38}$$

For unstable conditions

$$\frac{C_{\ell A}^2(1)}{C_{\ell A}^2(2)} = \frac{C_N^2(1)}{C_N^2(2)} = \left[\frac{h(2)}{h(1)}\right]^{4/3} . \tag{37}$$

For the results displayed in Table 1, period (a) shows that $(h(2)/h(1))^{4/3}$ agrees with $C_{\ell A}^2(1)/C_{\ell A}^2(2)$ within 2 percent; for period (b) the agreement is 4 percent. For

period (c) $(h(2)/h(1))^{2/3}$ agrees with $C^2_{\ell A}(1)/C^2_{\ell A}(2)$ to within 4 percent, as would be expected for neutral conditions.

Table 2 shows the same data with aperture averaging corrections added using Figures 15 and 16.

TABLE 2

	Period (a)	Period (b)	Period (c)
$C_{\ell A}$ at h(1)	0.442	0.425	0.324
$C_{\ell A}$ at h(2)	0.226	0.226	0.240
$(h(2)/h(1))^{4/3}$	3.44	3.44	
$(h(2)/h(1))^{2/3}$			1.85
$C^2_{\ell A}(1)/C^2_A(2)$	3.81	3.53	1.82

Period (a) shows agreement to 9.6 percent with the predictions for unstable conditions. Period (b) is within 2.5 percent of agreement with unstable conditions and period (c) is within 1.5 percent agreement with neutral stability conditions.

2. Optical Frequency Spectra

Figure 23 is a plot of relative power vs. frequency as seen by the two levels at 2134 (PDST) 18 October. The plot is very much like that of Figure 21 where the two detection systems were placed side by side. From equations (49), (50) and (51), the theoretical temporal frequency spectrum, W(f) is a function of $C^2_{\ell A}$, f_o, f and R. The

ratio W(f)/W(20Hz) varies only with f_o and f. For a given frequency, the relative power values are dependent on the effective magnitude of v at the sensor level. Figure 23 indicates that the value of v must have been comparable at the two levels on 18 October and less than v on 22 October.

3. Meteorological Measurements

As defined in Section II.B., when the surface temperature flux, Q, is positive, the air mass is unstable. Q equal to zero corresponds to neutral conditions and Q negative corresponds to stable conditions. The temperature difference between the sea water and the air at the lower level, 4.525 meters above the surface, is plotted in Figure 24. Conditions were unstable from 2105 to 2200 when the ship left the area. Although quantitative measurements of Q after 2200 were not available, low lying coastal clouds were setting in throughout the evening with a ceiling of 200-300 feet by 2220. The increasing cloudiness would tend to change conditions toward neutrality and the corresponding -2/3 relationship.

A malfunction in the lower level temperature probe system prevented the comparison of the two level optical data with meteorological data. The difference of 3.9 meters in the upper levels of the optical and meteorological sensors prevented a point by point comparison of C_N values.

V. SUMMARY AND CONCLUSIONS

A. APERTURE AVERAGING

Significant aperture averaging was observed in an enclosed laboratory for apertures less than the first Fresnel zone size. Two field experiments, conducted under different turbulence conditions, indicated aperture averaging, for small apertures, is dependent on C_N. Data collected by Fried, Mevers and Keister [Ref. 7] lends support to this conclusion. Both field experiments show that a 4.8 mm aperture can approximate a vanishingly small receiver and should be used whenever possible. None of the existing theories adequately describe the observed data.

Application of a primitive method of predicting $C_{\ell A}(0)$ from $C_{\ell A}$ observed by a 23 mm collection aperture appeared to be successful for the two level experiment data. Additional aperture averaging data is required to make accurate predictions of $C_{\ell A}(0)$. The capability to make such predictions would greatly reduce the intensity per unit area required to collect good scintillation data.

The observed frequency spectrum is in general agreement with the predicted trends in Clifford's model for a spherical wave [Ref. 31] and Tatarski's aperture averaging modification term as applied to a plane wave [Ref. 2]. The effect of smaller apertures seeing more relative power in the higher frequencies than larger apertures was observed. For

the range of apertures used (3mm to 23 mm) the effect of aperture size on relative power at a given frequency was seen to be much less than the v dependence. An increase in v shows up as an increase in relative power in the higher frequencies.

B. DEPENDENCE OF SCINTILLATION ON HEIGHT

Wyngaard, Izumi and Collins [Ref. 16] predicted C_N^2 was dependent on $h^{-4/3}$ for unstable meteorological conditions and on $h^{-2/3}$ for neutral meteorological conditions in the context of long time averages, near the surface, over land. The data presented in Tables 1 and 2, though sparse, are in excellent agreement with these predictions and indicate that the semi-empirical theory is applicable to propagation paths over the ocean surface.

C. EXPERIMENTAL PROCEDURE

Accumulation of scintillation data for the aperture averaging experiments and the two level experiment pointed out some potential sources of error. Beam wander makes a significant contribution to the scintillation observed by a detector. If meteorological measurements are to be used to predict the amount of scintillation a laser beam experiences, an additional term should be found to compensate for the effect of beam wander.

The value of C_N is strongly dependent on the height of the propagation path. This fact can be used to obtain large ranges of C_N on any given day. When making comparisons

of C_{NO} and C_{NT} care should be taken to ensure all optical components and meteorological sensors are on the same level because the -4/3 and -2/3 scaling laws are not applicable to short time average comparisons.

Figure 1

(Log-Amplitude Covariance)$^{1/2}$ vs. Aperture Diameter.

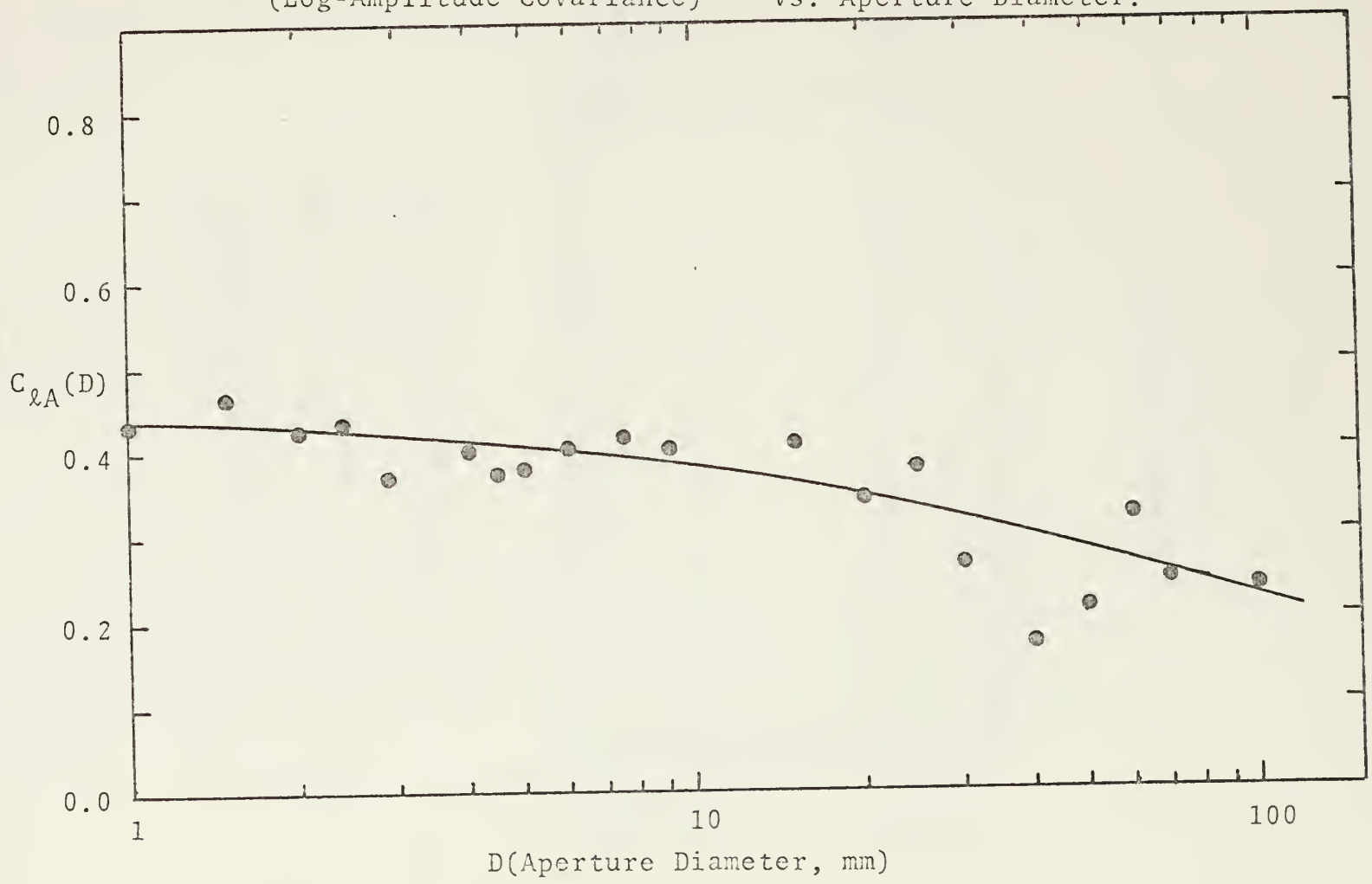

(after Fried, Mevers and Kiester [Ref. 7])

Figure 2

Scintillation

Detector Package

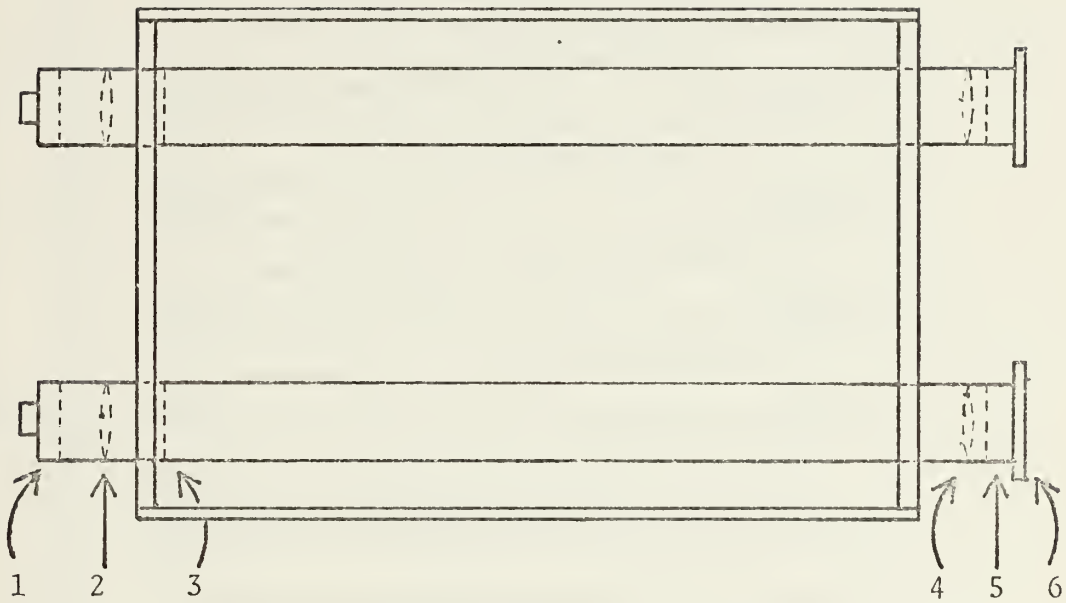

1. Pin 10 Silicon Photodiode
2. Field Lens
3. Field Limiting Aperture
4. Objective Lens
5. 10 A Narrow-Band Filter Centered at 6328 A
6. 18 Leaf Iris

Figure 3

Pin 10 Photodiode Relative Intensity Response (I) vs. Position on Surface.

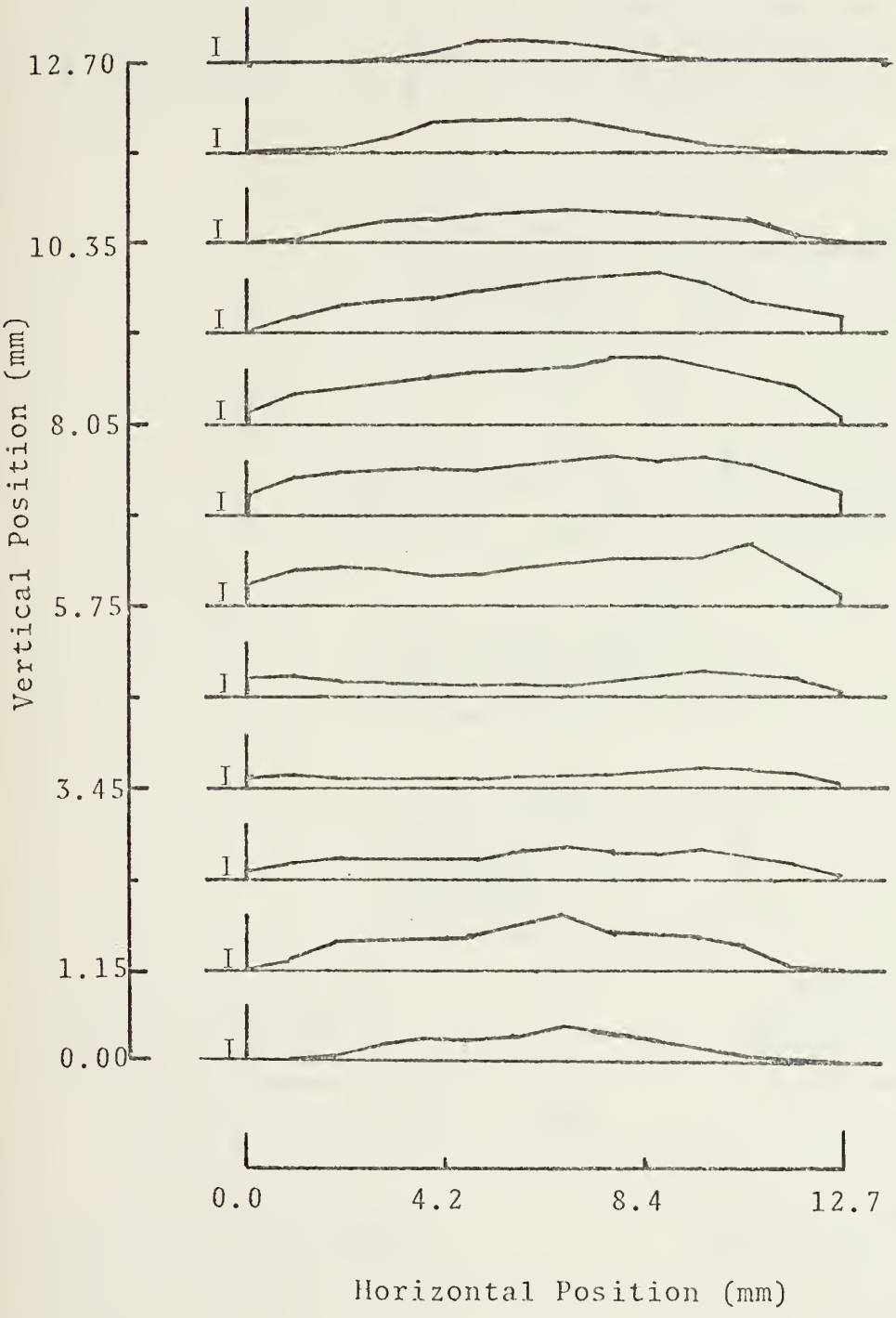

Figure 4

Scintillation Measurement Electronic Components

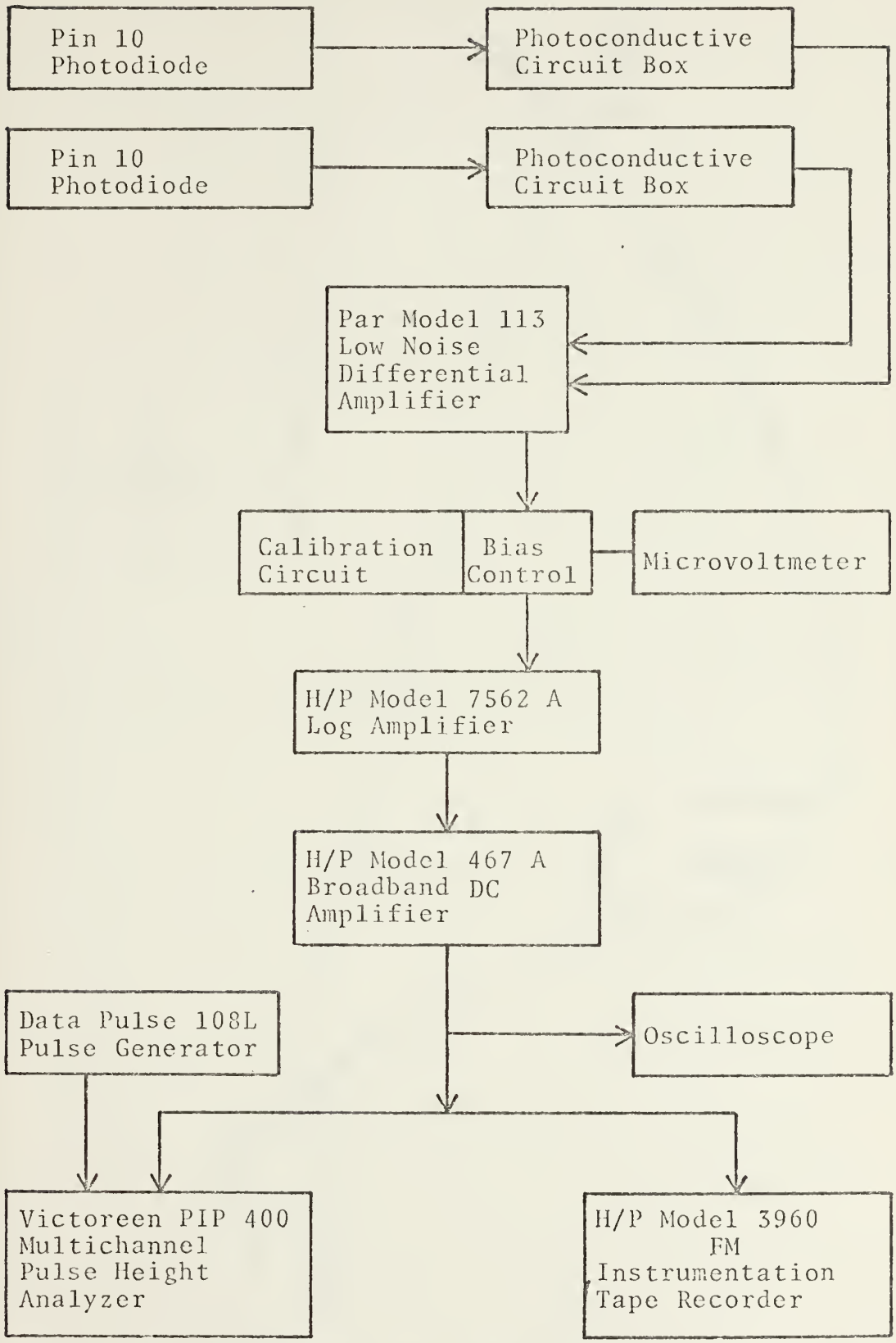

Figure 5

Experimental Propagation Path

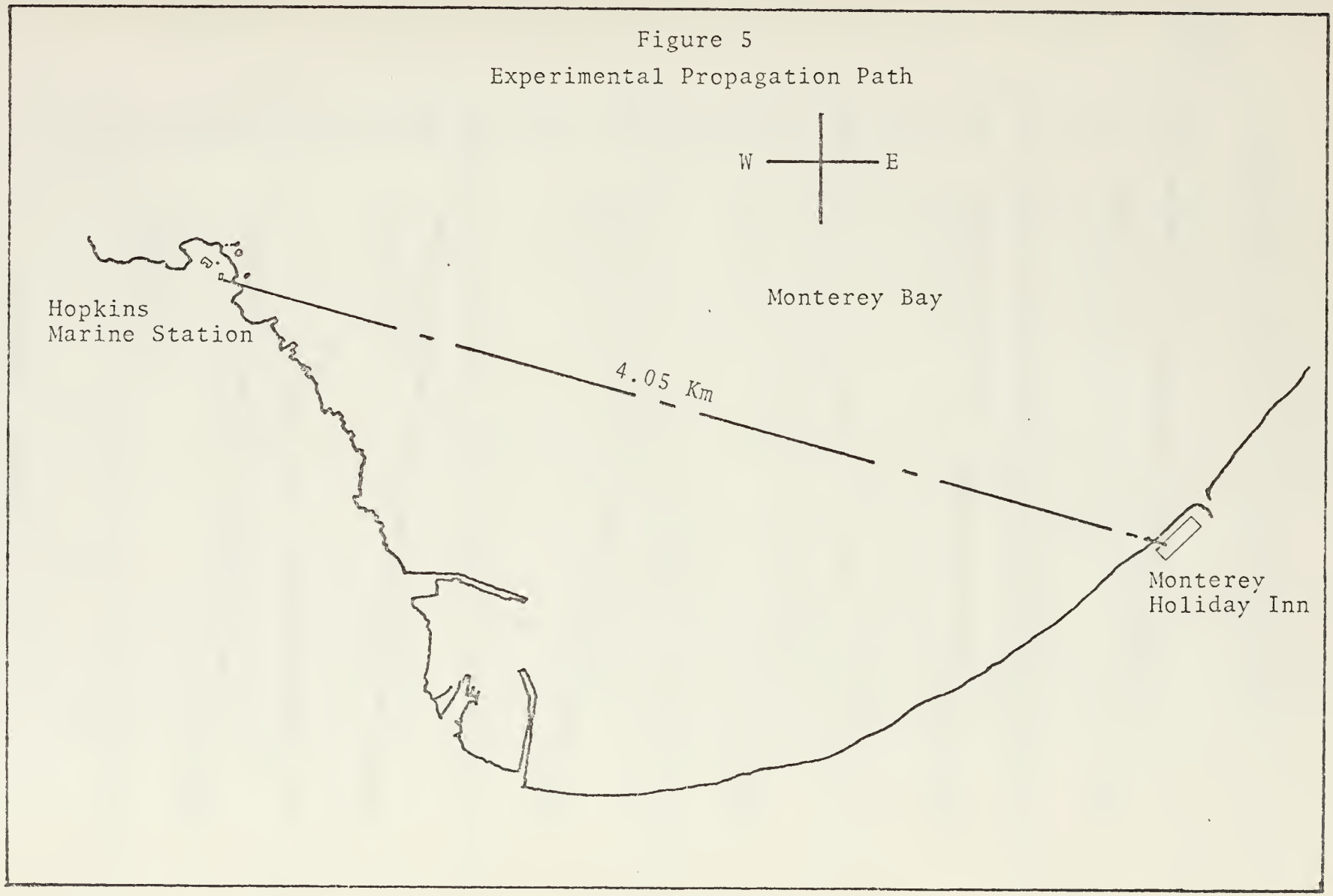

Figure 6

Laboratory Aperture Averaging Experiment

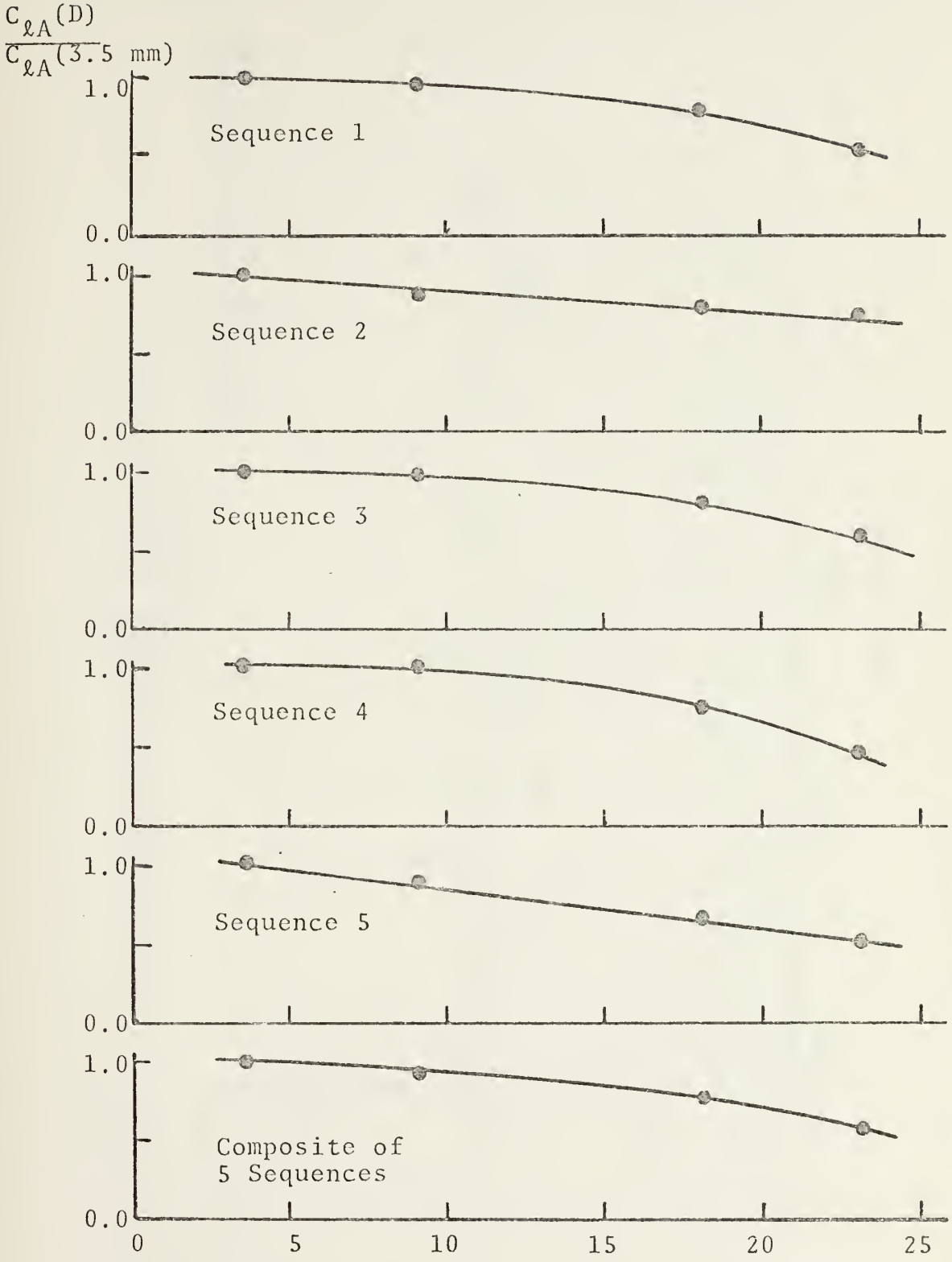

Figure 7
[Log Amplitude Covariance (Using 23 mm Aperture)]$^{1/2}$
vs. Time
22 October 1973

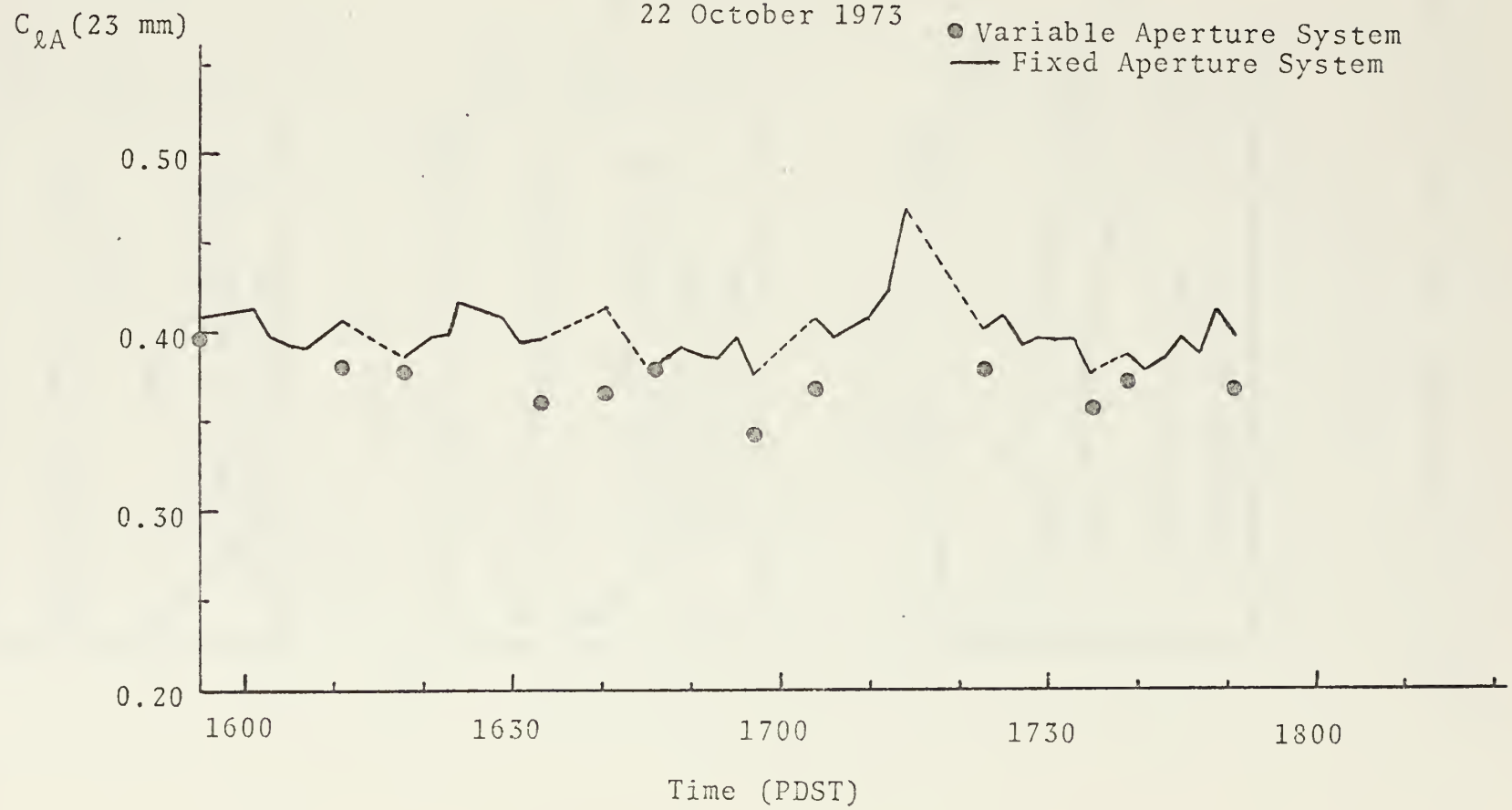

Note: $C_N = 1.162 \times 10^{-7} C_{\ell A}$

Figure 8

$[\text{Log Amplitude Covariance (Using Aperture D)}]^{1/2}$

vs. Time

22 October 1973

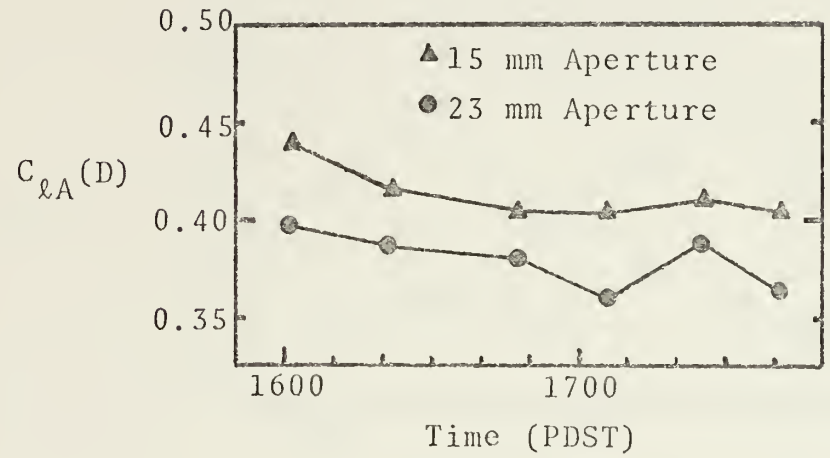

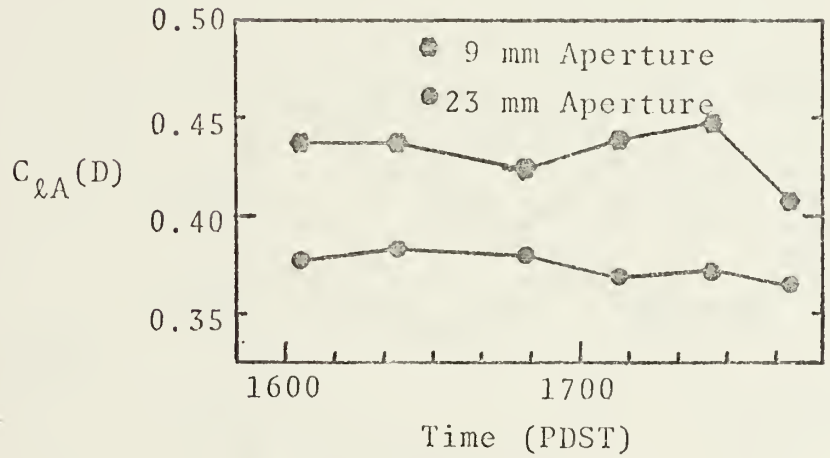

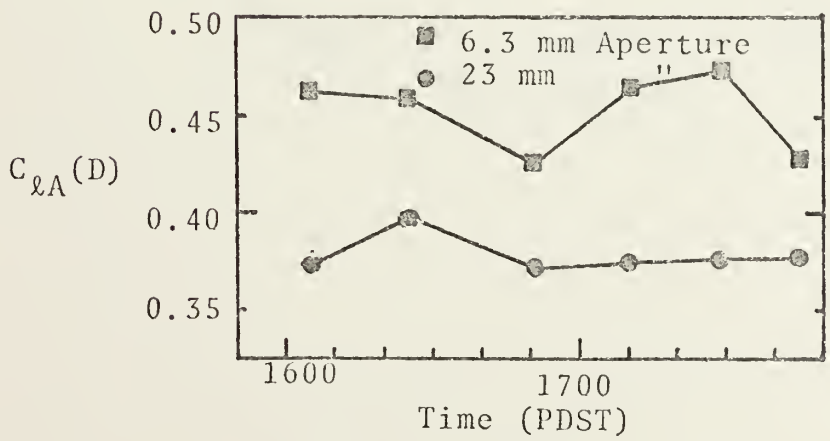

Figure 9

[Log Amplitude Covariance (Using Aperture D)]$^{1/2}$

vs. Time

22 October 1973

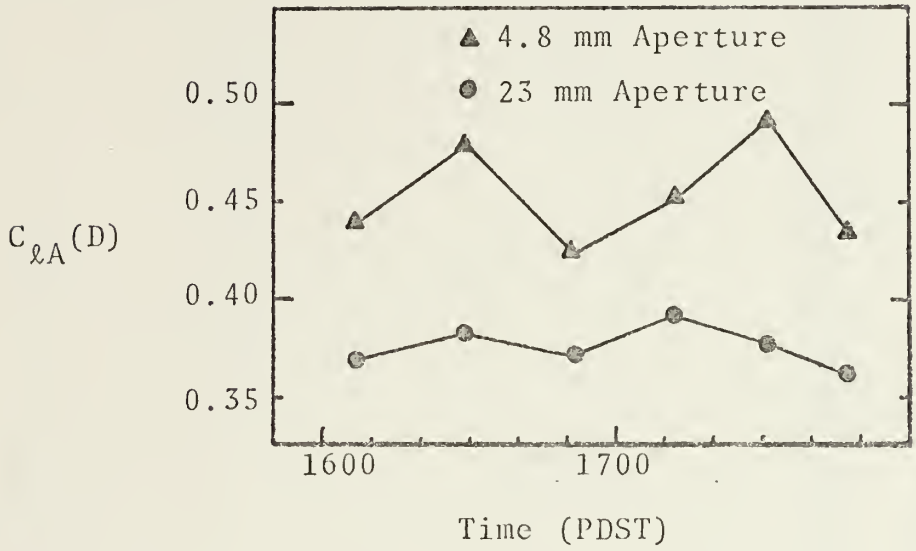

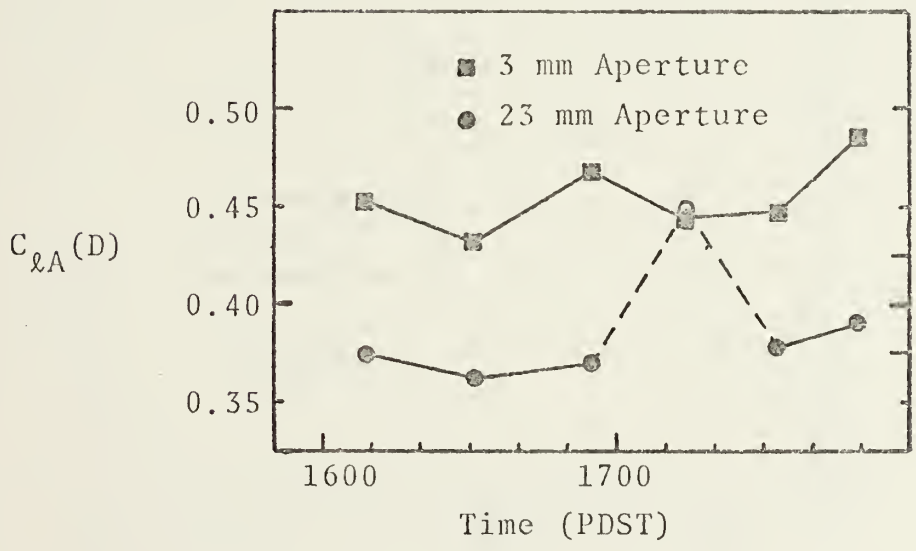

Figure 10

$\langle C_{\ell A}(D) - C_{\ell A}(23\ mm)\rangle$ vs. Aperture Diameter

22 October 1973

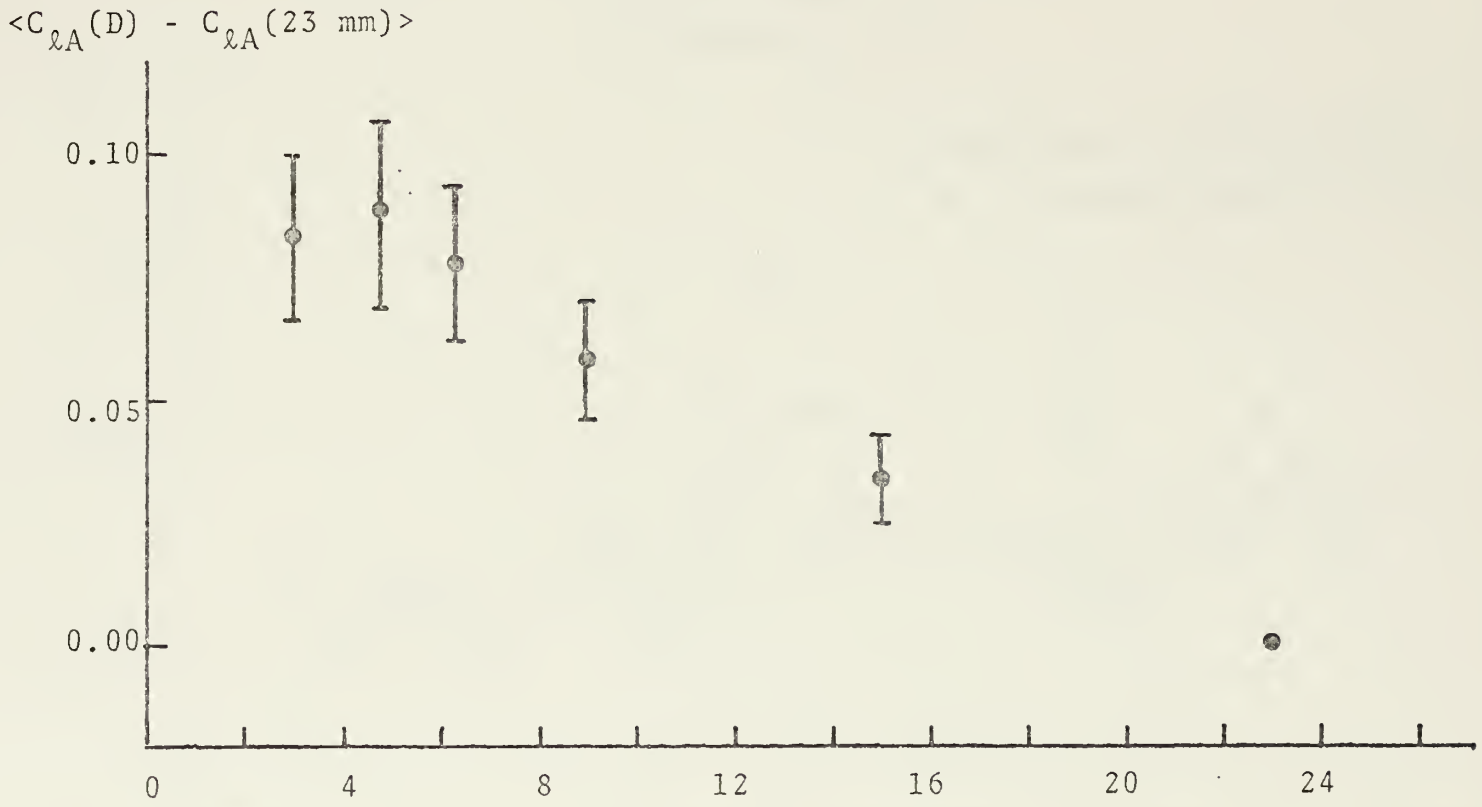

$\langle C_{\ell A}(D) - C_{\ell A}(23\ mm)\rangle$ is the average value of the difference in the square roots of the log amplitude variance as sensed through aperture diameter D and through a 23 mm aperture.

Figure 11

[Log Amplitude Covariance (Using 23 mm Aperture)]$^{1/2}$

vs. Time

27 September 1973

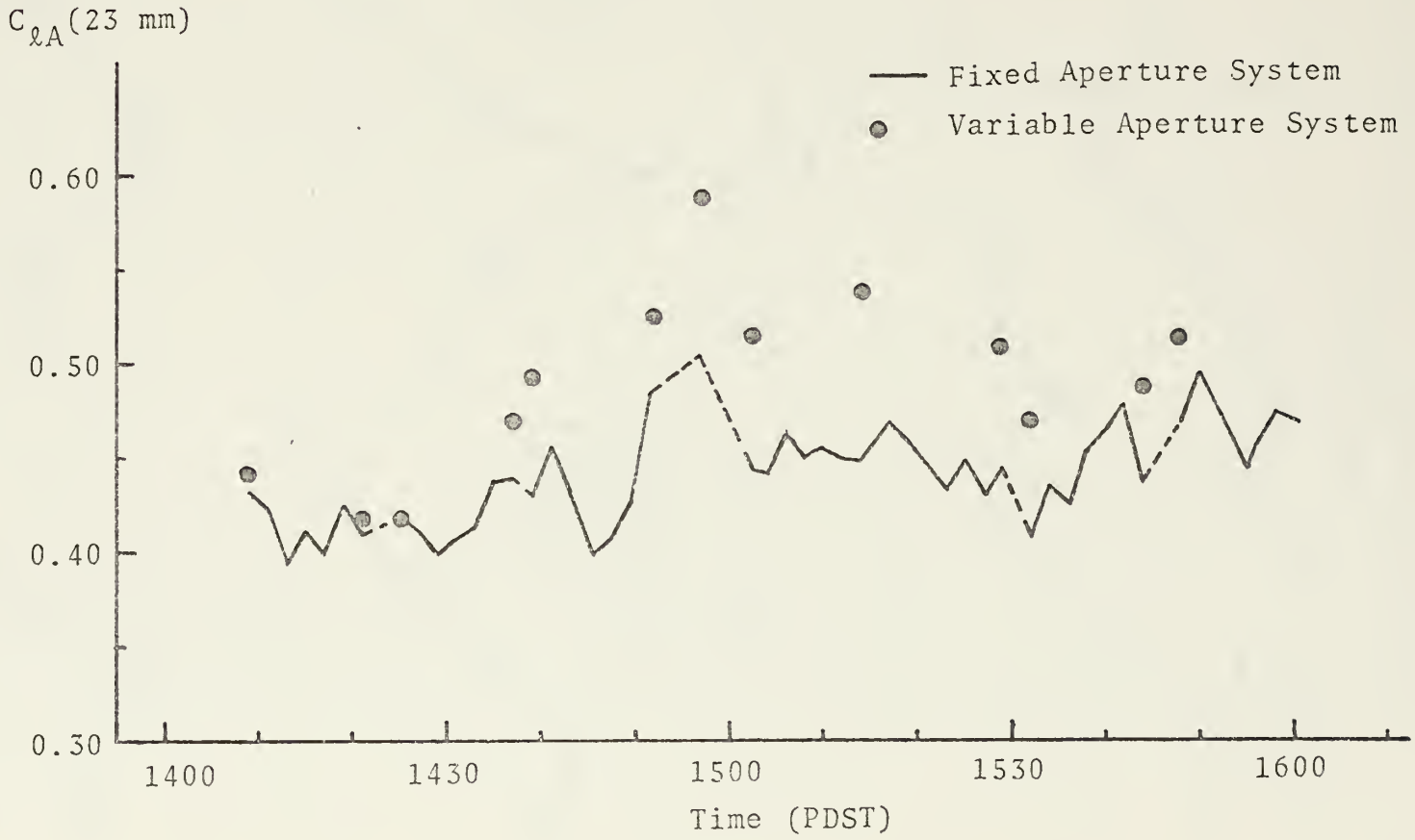

Note: $C_N = 1.162 \times 10^{-7} C_{\ell A}$

Figure 12

[Log Amplitude Covariance (Using Aperture D)]$^{1/2}$
vs. Time
27 October 1973

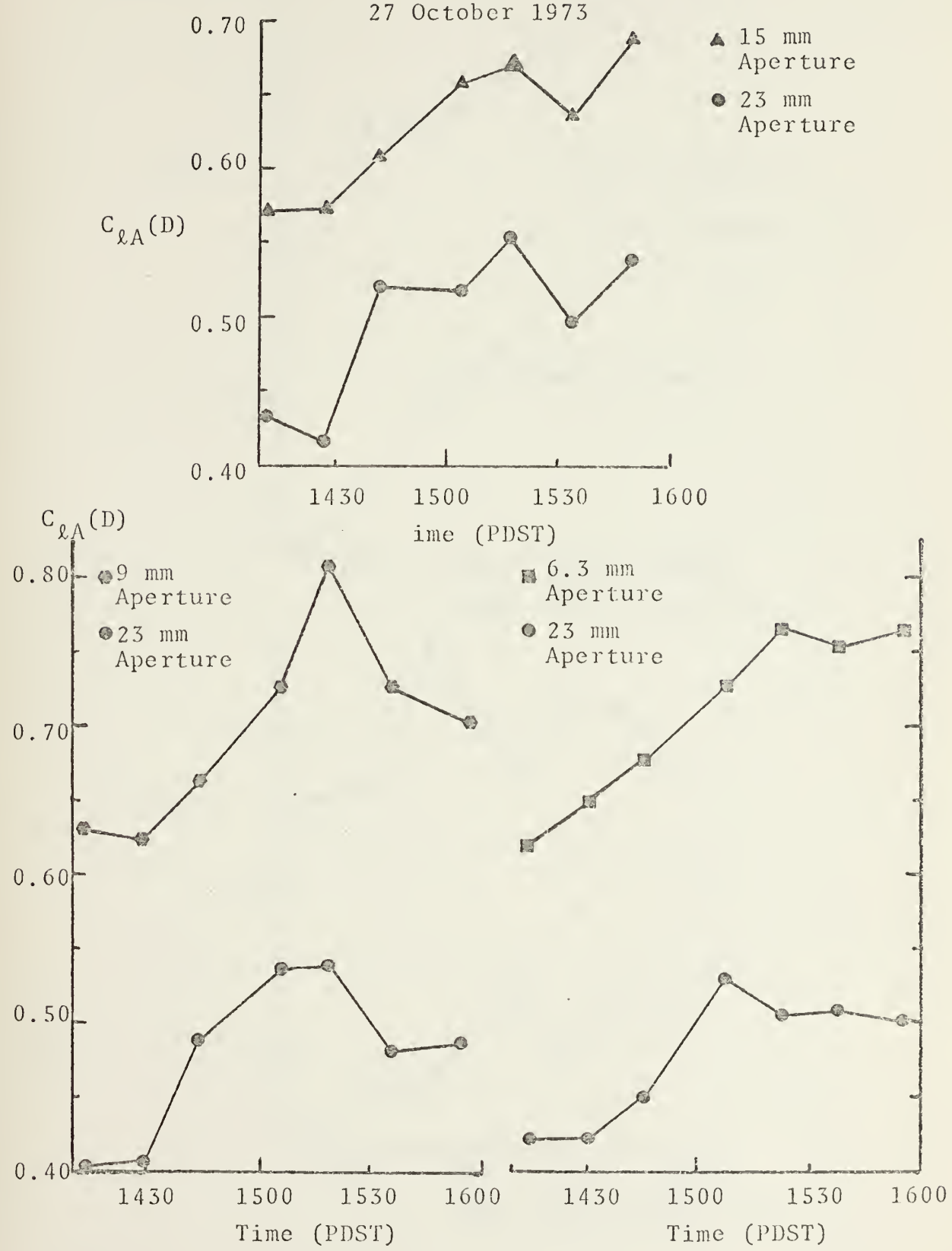

Figure 13
[Log Amplitude Covariance (Using Aperture D)]$^{1/2}$
vs. Time

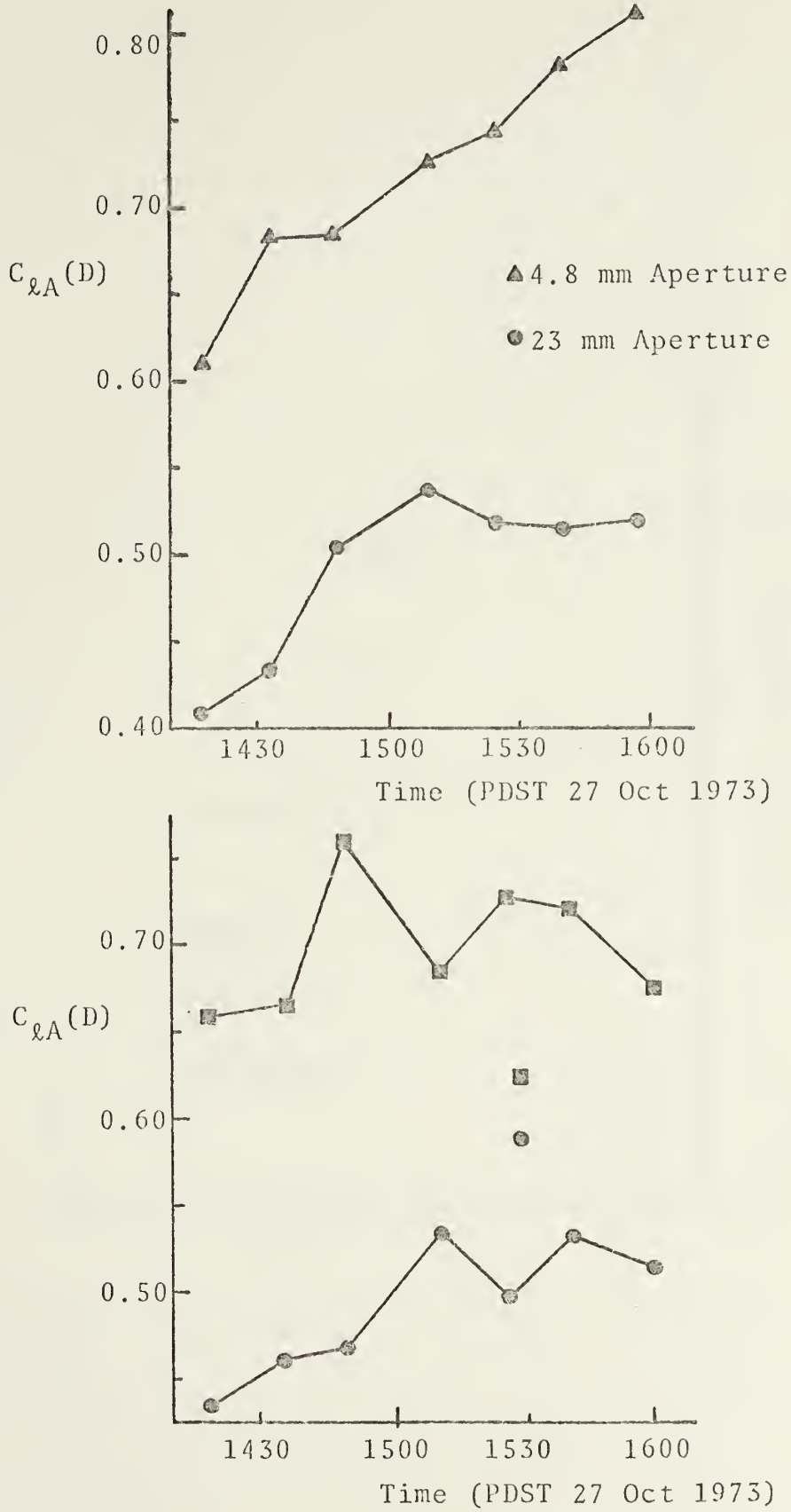

Figure 14

$\langle C_{\ell A}(D) - C_{\ell A}(23\ mm)\rangle$ vs. Aperture Diameter

27 October 1973

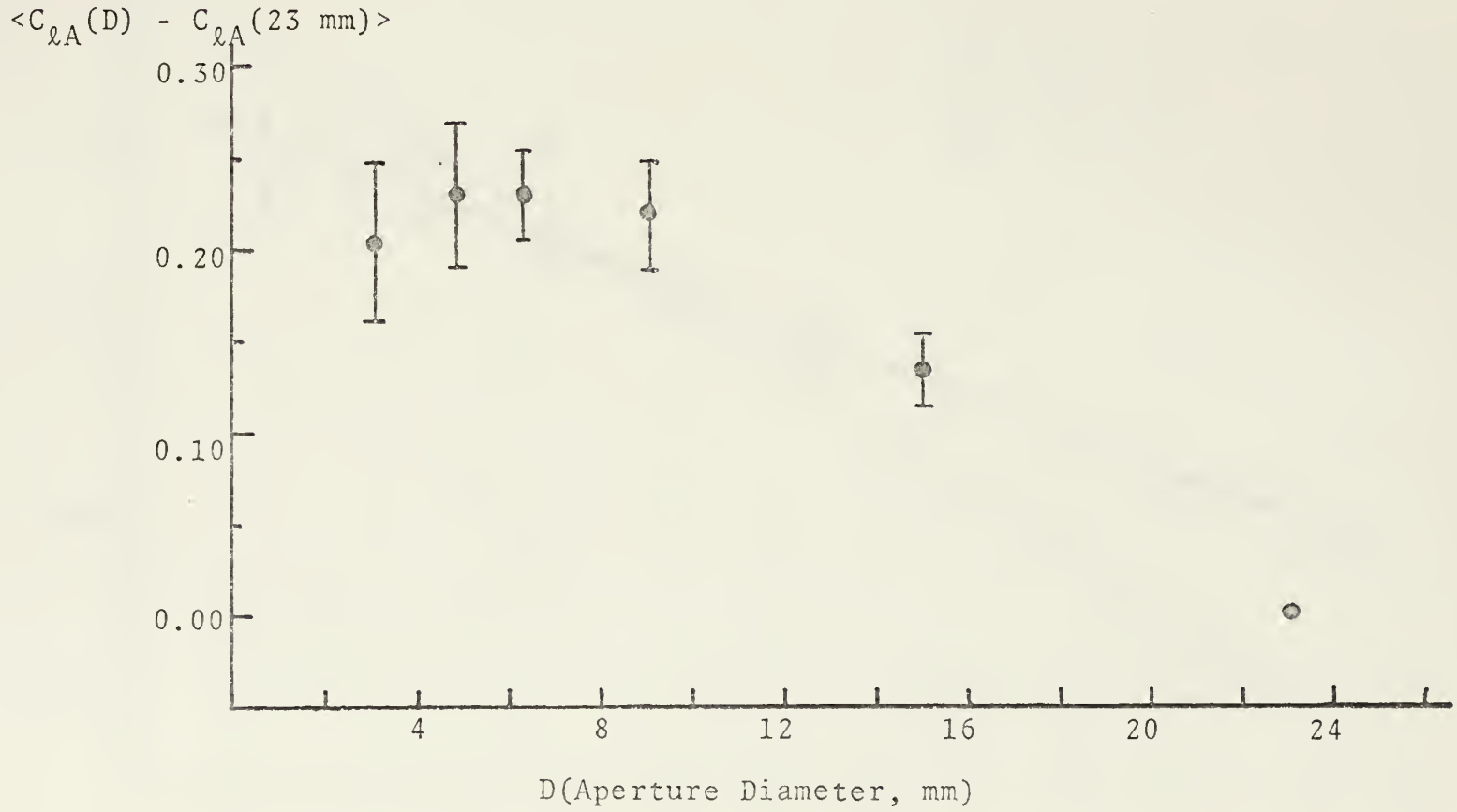

$\langle C_{\ell A}(D) - C_{\ell A}(23\ mm)\rangle$ is the average value of the difference in the square roots of the log amplitude variance as sensed through aperture diameter D and through a 23 mm aperture.

Figure 15

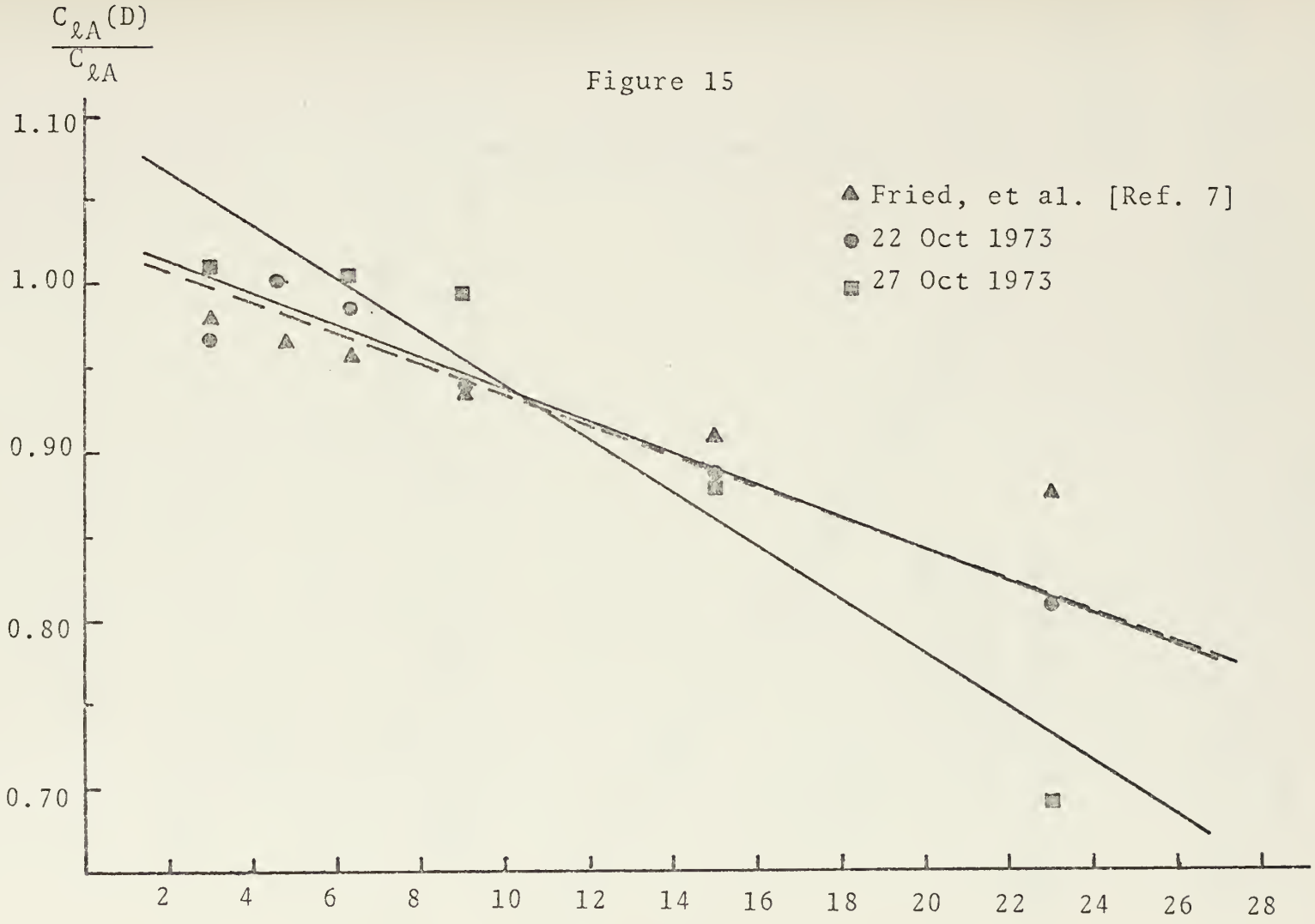

The Square Root of the Normalized Log Amplitude Covariance (D) vs. Aperture Diameter

Figure 16

[Log Amplitude Covariance (Using 23 mm Aperture)]$^{1/2}$

vs.

The Inverse Slope of Regression Lines Plotted in Figure 15.

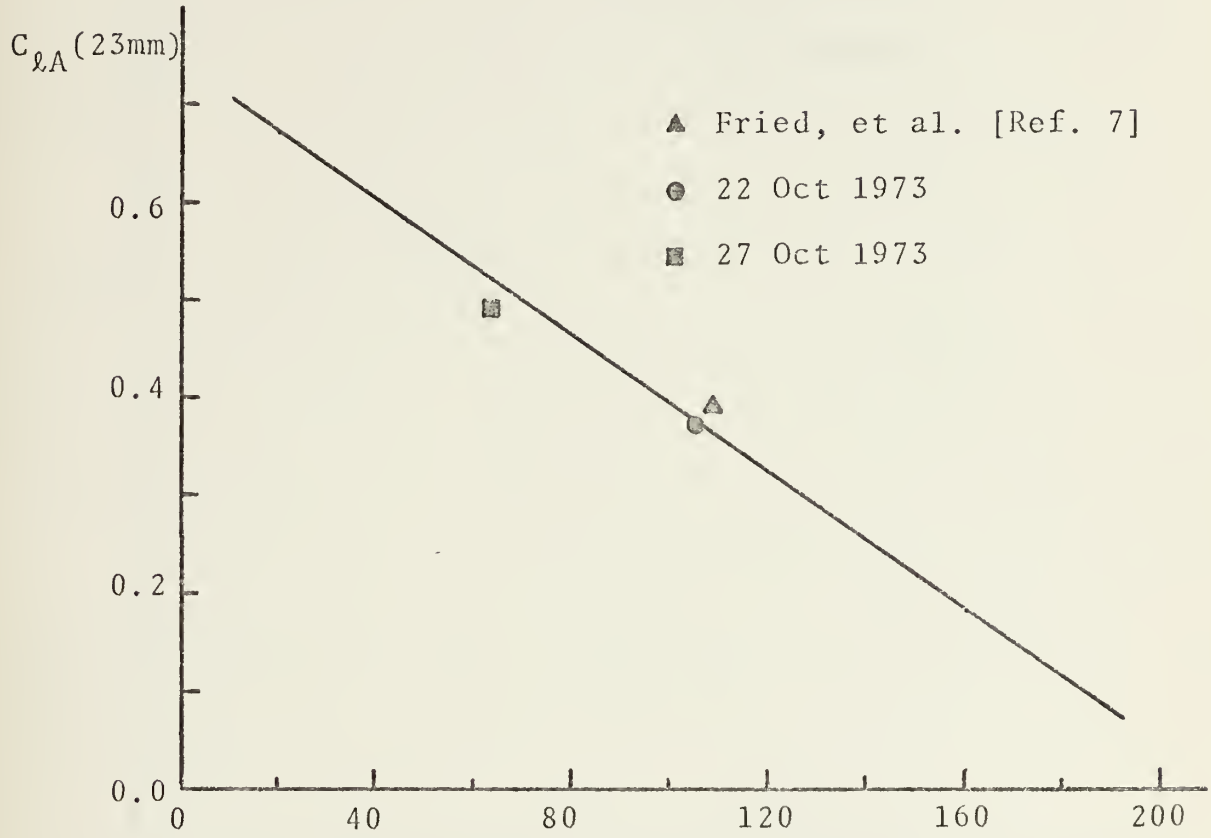

Figure 17

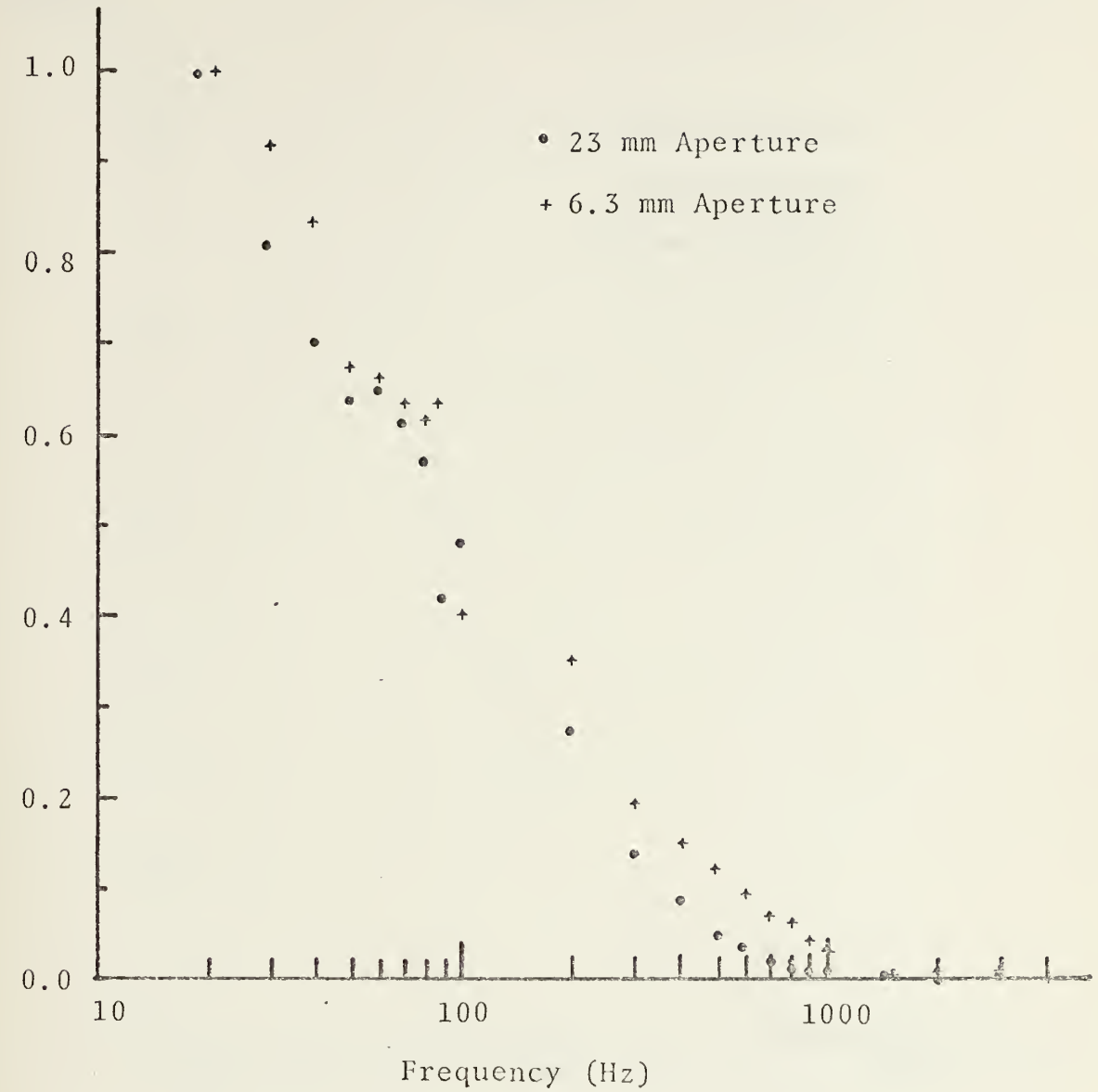

Relative Spectral Power [W(f)/W(20Hz)]
vs. Frequency.

Figure 18

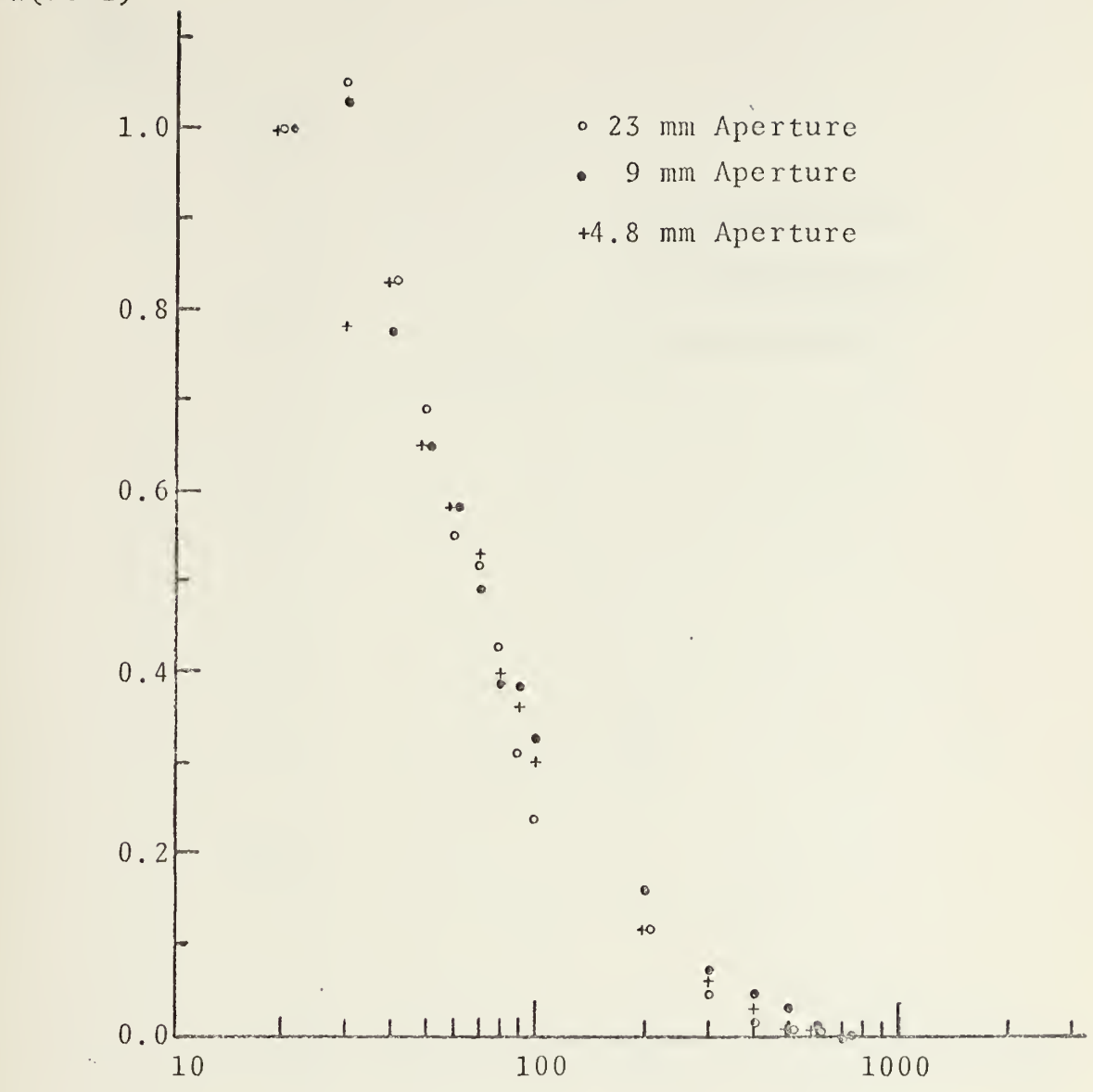

Relative Spectral Power [W(f)/W(20Hz)]
vs. Frequency.
for 23 mm, 9 mm and 4.8 mm Apertures.

Figure 19

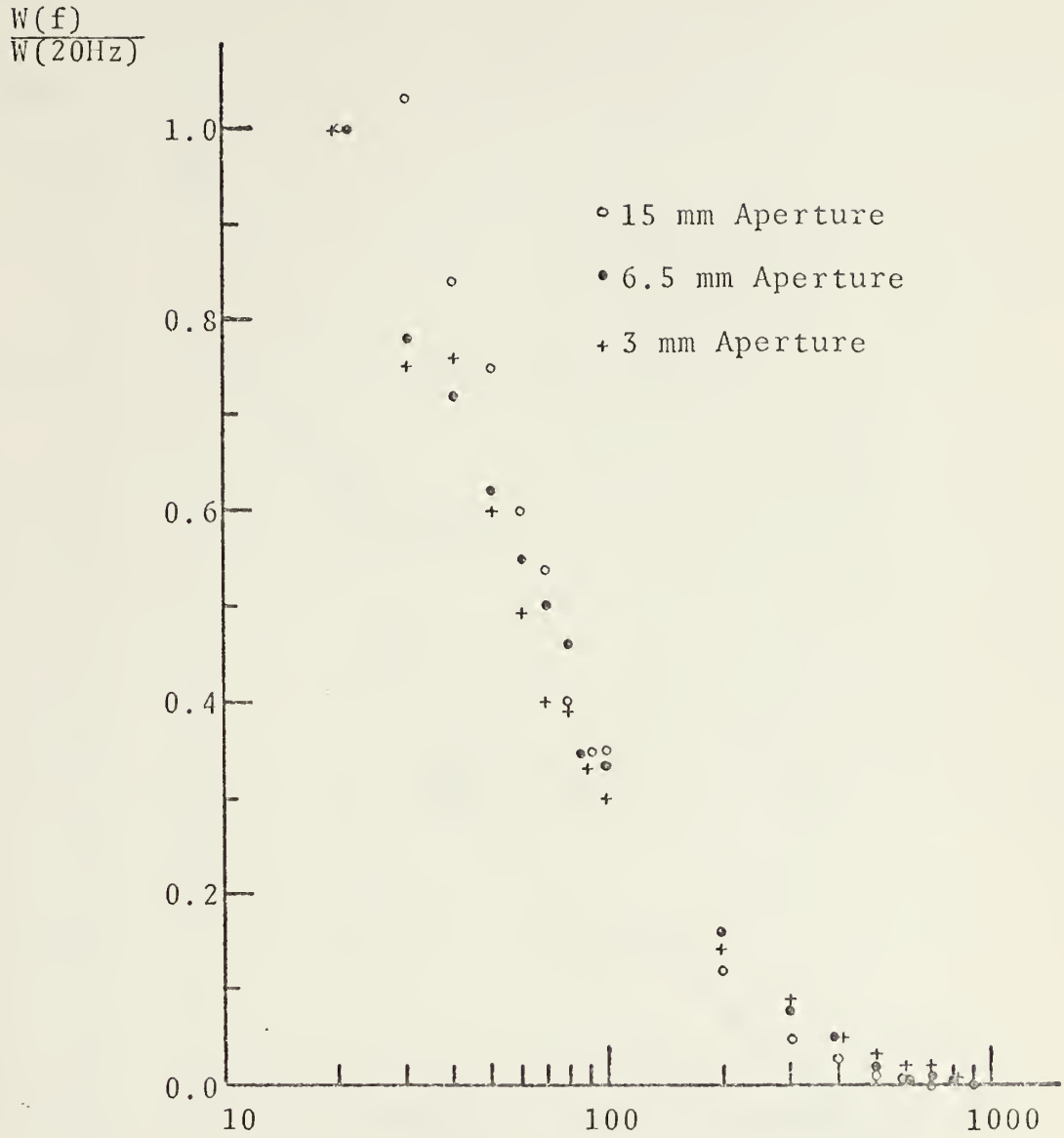

Relative Spectral Power [W(f)/W(20Hz)]
vs. Frequency
for 15 mm, 6.3 mm and 3 mm Apertures.

Figure 20

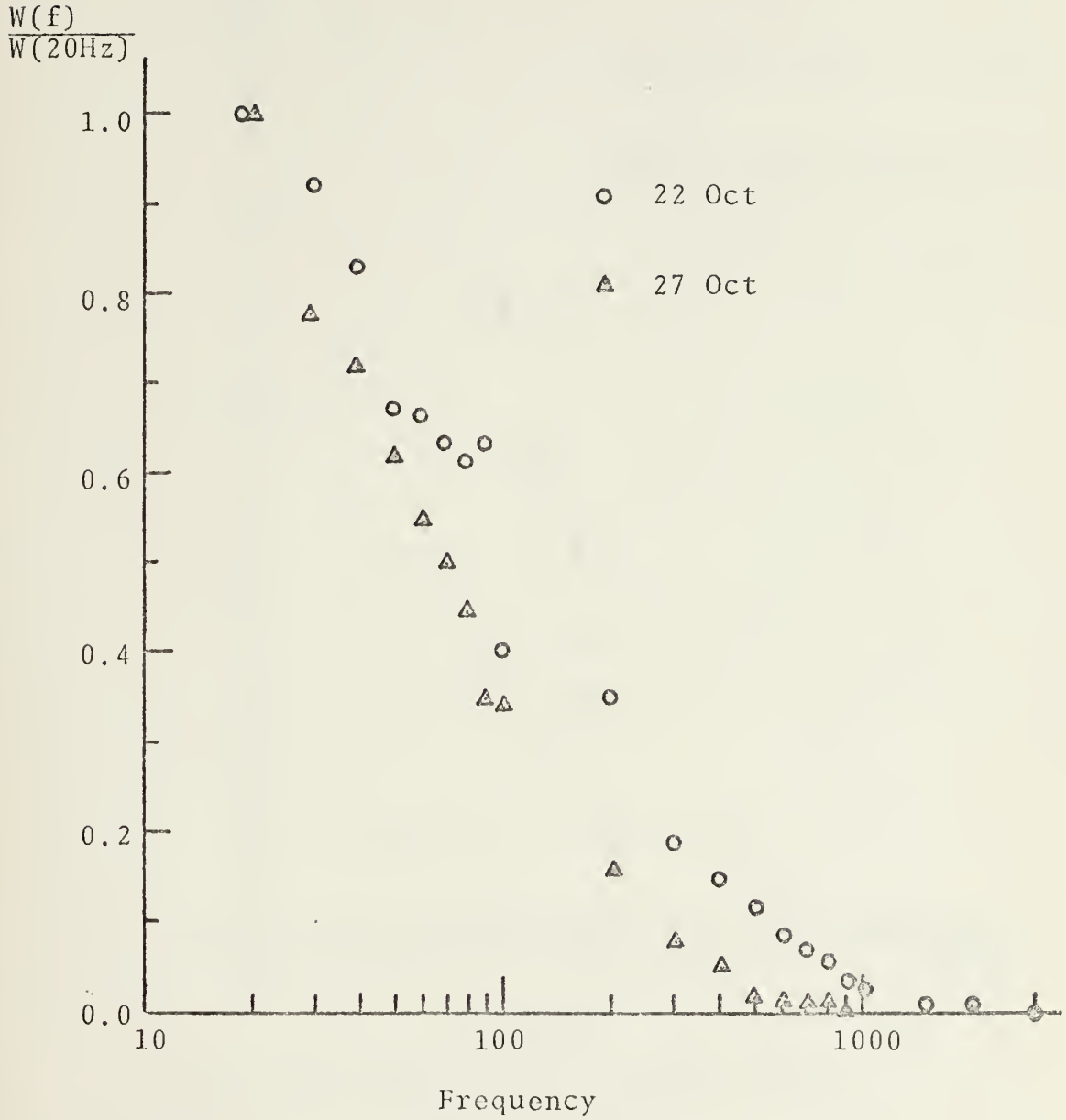

Relative Spectral Power [W(f)/W(20Hz)]
vs. Frequency
for a 6.3 mm Aperture.

Figure 21

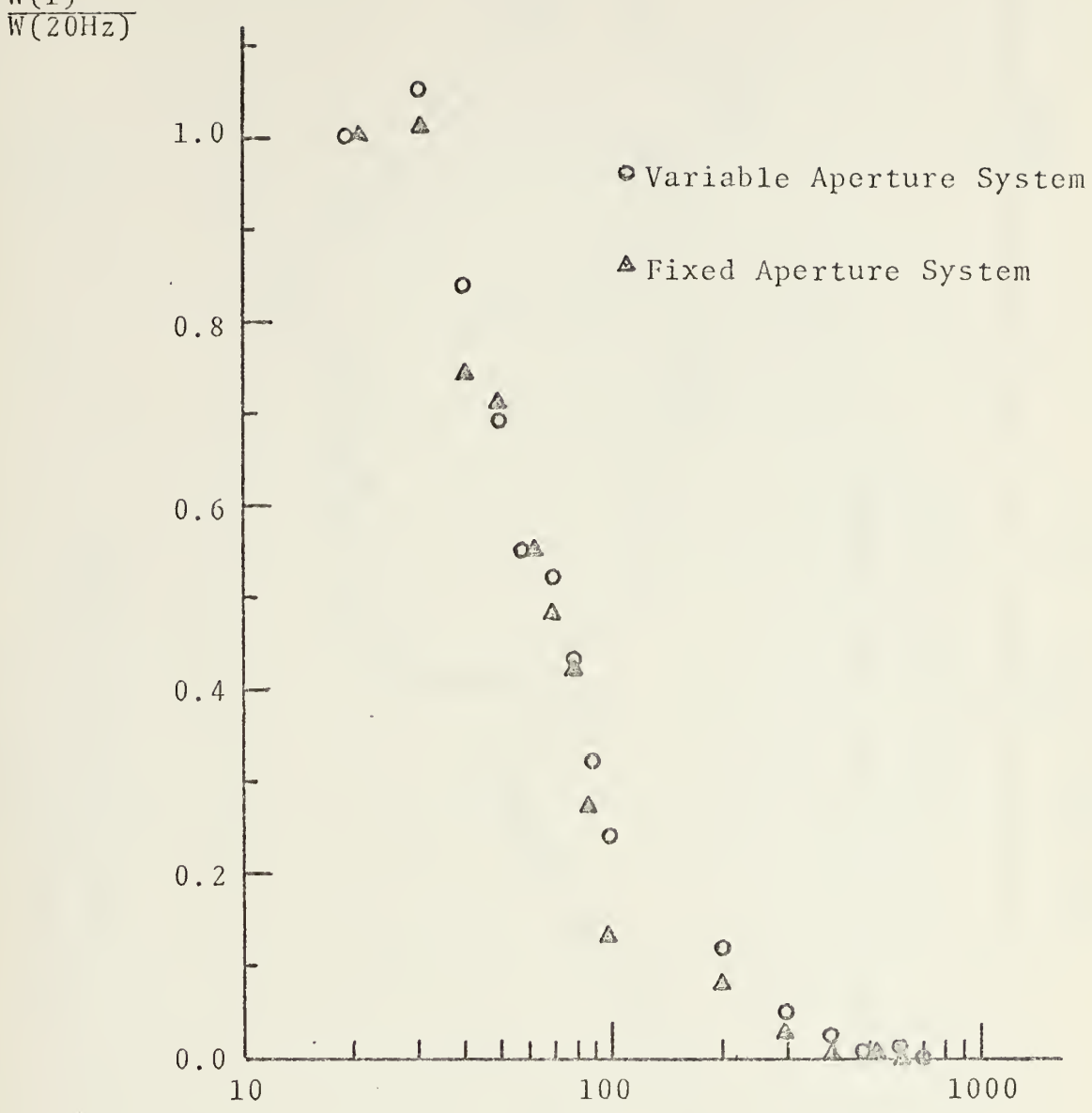

Relative Spectral Power [W(f)/W(20Hz)]
vs. Frequency
for 23 mm apertures, simultaneously
measured using fixed and variable
aperture systems.

Figure 22
[Log Amplitude Covariance]$^{1/2}$ vs. Time
Observed at Two Heights

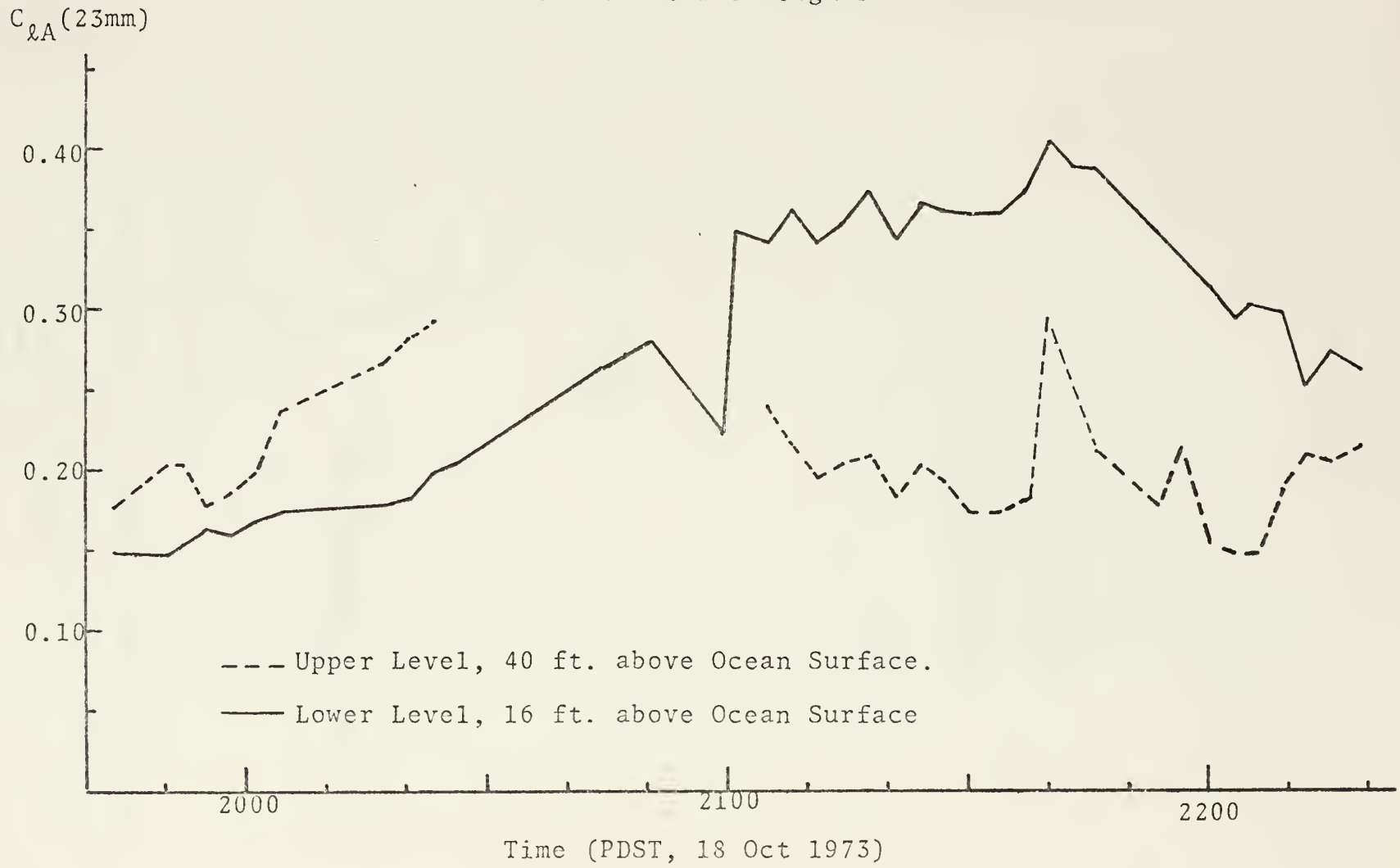

Figure 23

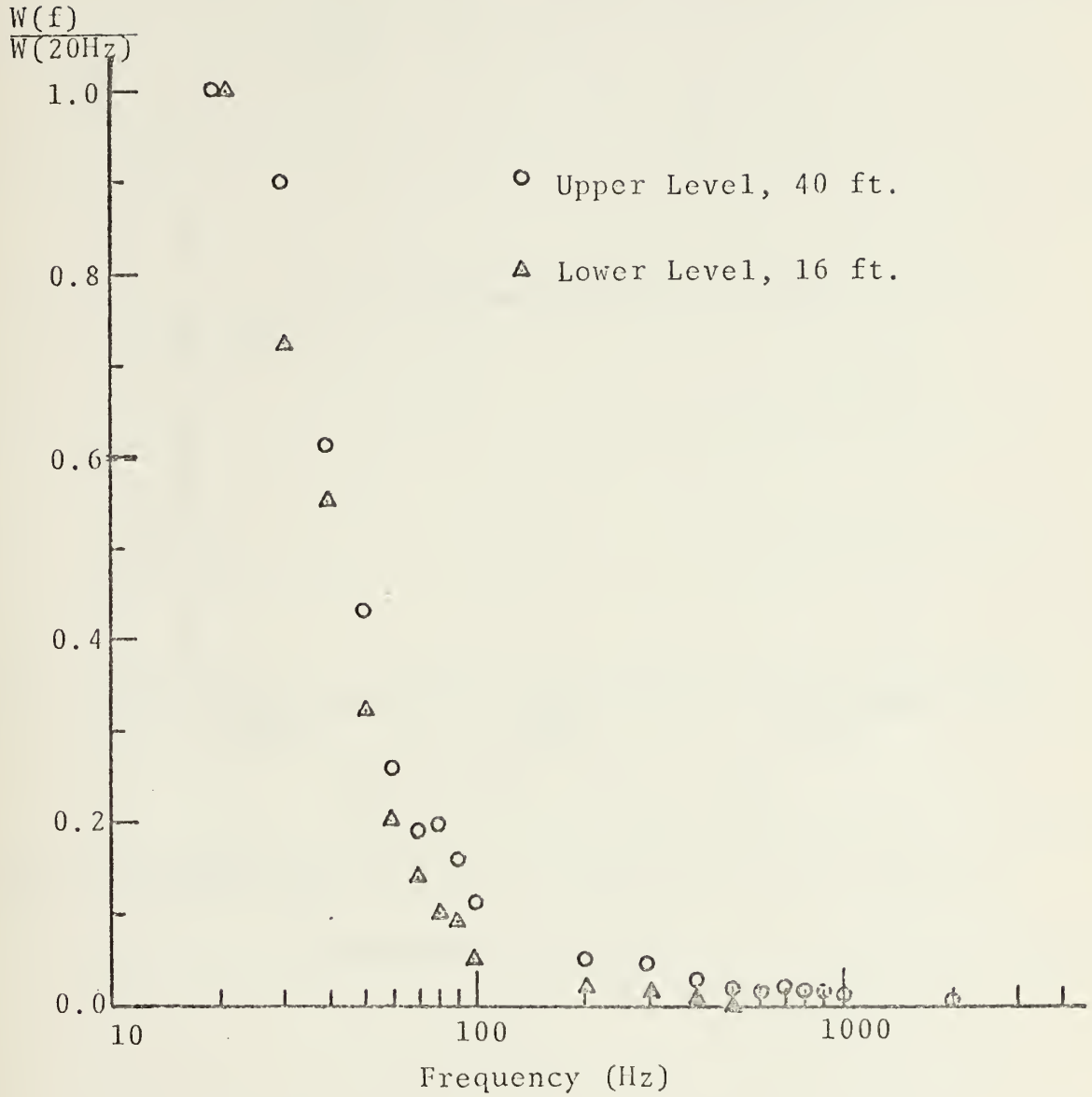

Relative Spectral Power [W(f)/W(20Hz)]
vs. Frequency

Observed at two heights above the ocean surface; the upper level utilized the variable aperture system, the lower level utilized the fixed aperture system (Aperture size, 23 mm).

Figure 24

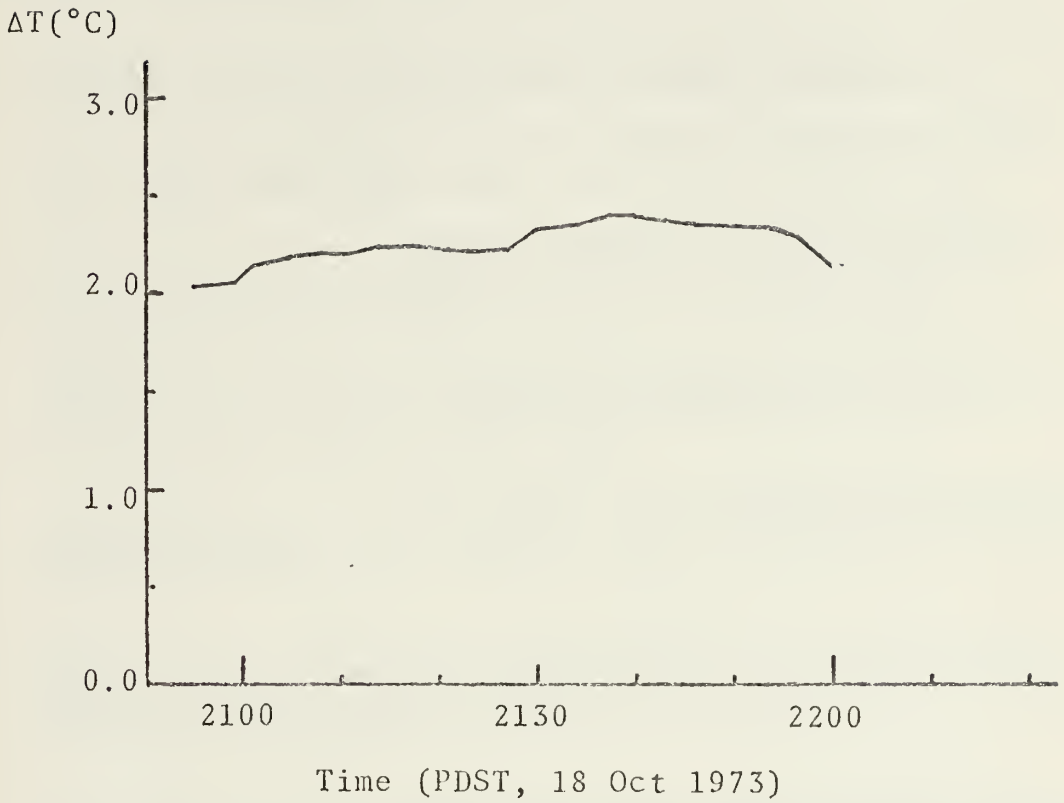

The Air Temperature at 14.7 ft. minus the Ocean Surface Temperature vs. Time.

BIBLIOGRAPHY

1. Kolmogoroff, A. Turbulence, Classical Papers on Statistical Theory, Friedlander, S. K. and Topper, L. Eds., p 151 Wiley, 1961.

2. Tatarski, V. I., The Effects of the Turbulent Atmosphere on Wave Propagation, National Science Foundation, 1971.

3. Rytov, S. M. "Diffraction of Light by Ultrasonic Waves" Izv. Akad. Nauk SSSR, Ser. Fiz., No 2 p 233, 1937.

4. Schmeltzer, R. A. "Means, Variances and Covariances for Laser Beam Propagation through a Random Medium," Quarterly Applied Math, Vol 24, p 339-354, 1967.

5. Fried, D. L., "Laser-Beam Scintillation in the Atmosphere," Journal of the Optical Society of America, Vol 57, No. 2, p 181-185, February 1967.

6. Haagensen, B. C., Laser Beam Scintillation in the Marine Boundary Layer, M.S. Thesis, Naval Postgraduate School, Monterey, 1973.

7. Fried, D. L., Mevers, G. E., and Keister, M. P. "Measurements of Laser-Beam Scintillation in the Atmosphere," Journal of the Optical Society of America, Vol. 57, No. 6, p 787-797, June 1967.

8. Hildebrand, W. T., An Optical Apparatus to Determine the Effect of Turbulence on the Modulation Transfer Function of the Atmosphere, M. S. Thesis.

9. Beall, D. A., An Experiment to Measure Laser Beam Wander and Beam Spread in the Marine Boundary Layer near Shore, M. S. Thesis, Naval Postgraduate School, Monterey, 1973.

10. Fried, D. L., "Aperture Averaging of Scintillation," Journal of the Optical Society of America, Vol 57, No. 2, p 169-175, February 1967.

11. Young, A. T., "Aperture Filtering and Saturation of Scintillation," Journal of the Optical Society of America, Vol 60, No. 2, p 248-250, February 1970.

12. Young, A. T., Astronomical Journal, Vol 72, p 747, 1967.

13. Young, A. T., "Photometric Error Analysis. VIII the Temporal Power Spectrum of Scintillation," Applied Optics, Vol 8, p 869, 1969.

14. Kerr, J. R., "Experiments on Turbulence Characteristics and Multiwavelength Scintillation Phenomena," Journal of the Optical Society of America, Vol 62, No. 9, p 1040-1049, September 1972.

15. Dunphy, J. R., and Kerr, J. R., "Scintillation Measurements for Large Integrated-Path Turbulence," Journal of the Optical Society of America, Vol 63, No. 8, p 981-986, Aug 1973.

16. Wyngaard, J. C., Izumi, Y., and Collins, S. A., Jr. "Behavior of the Refractive-Index-Structure Parameter near the Ground," Journal of the Optical Society of America, Vol 61, No. 12, p 1646-1650, Dec 1971.

17. Businger, J. A. and others, Journal of Atmospheric Science, Vol 28, p 181, 1971.

18. DeWolf, D. A., "Saturation of Irradiance Fluctuations due to Turbulent Atmosphere," Journal of the Optical Society of America, Vol 58, No. 4, p 461-466, Apr 1968.

19. Strohbehn, J. W., and Wang, T. I., "Simplified Equation for Amplitude Scintillations in a Turbulent Atmosphere," Journal of the Optical Society of America, Vol 62, No. 9, p 1061-1068, Sep 1972.

20. DeWolf, D. A., "Strong Irradiance Fluctuations in Turbulent Air: Plane Waves," Journal of the Optical Society of America, Vol 63, No. 2, p 171-179, Feb 1973.

21. Strohbehn, J. W., "Line of Sight Wave Propagation through the Turbulent Atmosphere," Proceedings of the IEEE, p. 1301-1317, Aug 1968.

22. Klyatskin, V. I., Soviet Physics JETP, Vol 33, p 703, 1971.

23. Yura, H. T., "Optical Propagation through a Turbulent Medium," Journal of the Optical Society of America, Vol 59, p 111, 1969.

24. Sancer, M. I., and Varvatsis, A. D., "Saturation Calculation for Light Propagation in the Turbulent Atmosphere," Journal of the Optical Society of America, Vol 60, p 654, 1970.

25. Taylor, L. S., and Torrieri, D. J., "Irradiance Fluctuations in Optical Transmission through the Atmosphere," Journal of the Optical Society of America, Vol 62, p 145, 1972.

26. Brown, W. P., Jr., "Fourth Moment of a Wave Propagating in a Random Medium," Journal of the Optical Society of America, Vol 62, No. 8, p 966-971, Aug 1972.

27. Lutomirski, R. F., and Yura, H. T., "Propagation of a Finite Optical Beam in an Inhomogeneous Medium," Applied Optics, Vol 10, p 1652, 1971.

28. Mitchell, R. L., "Permanence of the Log-Normal Distribution," Journal of the Optical Society of America, Vol 58, No. 9, p 1267-1272, Sep 1968.

29. Hammond, R. G., An Observational Study of the Refractive-Index-Structure Parameter over Ocean Waves, M. S. Thesis, Naval Postgraduate School, Monterey, California, September 1973.

30. Ho, T. L., "Log Amplitude Fluctuations of Laser Beam in a Turbulent Atmosphere," Journal of the Optical Society of America, Vol 59, No. 4, p 385-390, Apr 1969.

31. Clifford, S. F., "Temporal-Frequency Spectra for a Spherical Wave Propagating through Atmospheric Turbulence," Journal of the Optical Society of America, Vol 61, No. 10, p 1285-1292, Oct 1971.

INITIAL DISTRIBUTION LIST

		No. Copies
1.	Defense Documentation Center Cameron Station Alexandria, Virginia 22314	2
2.	Library, Code 0212 Naval Postgraduate School Monterey, California 93940	2
3.	Department Chairman, Code 61 Department of Physics and Chemistry Naval Postgraduate School Monterey, California 93940	2
4.	Assoc Professor A. W. Cooper, Code 61Cr Department of Physics and Chemistry Naval Postgraduate School Monterey, California 93940	8
5.	LCDR Arthur F. Schroeder, Jr., USN PSC 2 Box 2000 Kirtland AFB, New Mexico 87117	1

REPORT DOCUMENTATION PAGE		READ INSTRUCTIONS BEFORE COMPLETING FORM
1. REPORT NUMBER	2. GOVT ACCESSION NO.	3. RECIPIENT'S CATALOG NUMBER
4. TITLE (and Subtitle) Laser Scintillation Properties in the Marine Boundary Layer		5. TYPE OF REPORT & PERIOD COVERED Master's Thesis; December 1973 6. PERFORMING ORG. REPORT NUMBER
7. AUTHOR(s) Arthur Frederick Schroeder, Jr.		8. CONTRACT OR GRANT NUMBER(s)
9. PERFORMING ORGANIZATION NAME AND ADDRESS Naval Postgraduate School Monterey, California 93940		10. PROGRAM ELEMENT, PROJECT, TASK AREA & WORK UNIT NUMBERS
11. CONTROLLING OFFICE NAME AND ADDRESS Naval Postgraduate School Monterey, California 93940		12. REPORT DATE December 1973 13. NUMBER OF PAGES 85
14. MONITORING AGENCY NAME & ADDRESS(if different from Controlling Office) Naval Postgraduate School Monterey, California 93940		15. SECURITY CLASS. (of this report) Unclassified 15a. DECLASSIFICATION/DOWNGRADING SCHEDULE

16. DISTRIBUTION STATEMENT (of this Report)

Approved for public release; distribution unlimited.

17. DISTRIBUTION STATEMENT (of the abstract entered in Block 20, if different from Report)

18. SUPPLEMENTARY NOTES

19. KEY WORDS (Continue on reverse side if necessary and identify by block number)

Laser
Atmosphere
Scintillation

20. ABSTRACT (Continue on reverse side if necessary and identify by block number)

Intensity scintillation has been studied for a He-Ne (6328A) laser beam propagating over a 4.05 kilometer horizontal path in the marine boundary layer. The results fall in three areas. (1) The covariance of the logarithm of the laser beam amplitude increases significantly with decreasing detector aperture diameter for apertures less than the first Fresnel zone size. This effect appears to be dependent on

the magnitude of the refractive index structure constant, C_N. (2) The dependence of C_N on (height)$^{-4/3}$ for unstable meteorological conditions was verified using the laser beam in determining C_N. (3) Frequency analysis performed on scintillation data indicates that the increase of power in higher frequencies is more dependent on the wind velocity perpendicular to the propagation path than on detector aperture diameter for apertures smaller than the first Fresnel zone size.